Probabilistic forecasts of temperature and precipitation change by combining results from global and regional climate models (CES Climate Modelling and Scenarios Deliverable D2.3)

Jouni Räisänen* and Leena Ruokolainen
Department of Physics, P.O. Box 48, FI-00014 University of Helsinki, Finland

18 August 2009

*Corresponding author
Email: jouni.raisanen@helsinki.fi

AVAILABLE FROM:
http://www.atm.helsinki.fi/~jaraisan/CES_D2.3/CES_D2.3.html

Table of Contents

Abstract

Probabilistic forecasts of temperature and precipitation change from the baseline period 1961-1990 to the scenario period 2021-2050 are constructed. The forecasts are based on a new method that combines large-scale information from 19 global climate model (GCM) simulations with small-scale information from 13 regional climate models (RCM) simulations, and takes into account the effects of both model differences and natural climate variability. Only simulations based on the A1B emission scenario are included in the analysis; however, previous work has shown that, in the first half of the 21^{st} century, differences between emission scenarios are still small compared with other sources of uncertainty.

The climate change forecasts derived with the new method are remarkably similar to those based on GCM data alone. The inclusion of RCM-based information adds credible small-scale detail to the projections, in particular near land-sea boundaries and in areas of high orography, but this systematic effect is generally small compared with the total uncertainty in future climate change.

The report consists of two parts, with somewhat different aims. In the first part, which is mainly directed to the more technically oriented readers, the new method for combining GCM and RCM results is described and its impact on projections of climate change is studied. In the second part, which may be more useful for readers from outside the climate modelling community, the derived probabilistic forecasts of temperature and precipitation change are presented in map format and their interpretation is briefly discussed.

1. Introduction

Despite the strong scientific consensus that increases in atmospheric greenhouse gases will lead to substantial changes in the global climate during this century (IPCC 2007), estimates of the magnitude (and for some aspects of climate, the direction) of the forthcoming changes are uncertain. This uncertainty comes from three basic sources:

- **Scenario uncertainty**: future changes in the atmospheric composition, and thus the external forcing of the climate system, depend on the magnitude of future anthropogenic emissions of greenhouse gases and other radiatively active substances such as aerosol particles and their precursor gases.
- **Modelling uncertainty** that results from our incomplete understanding, and incomplete capability to describe in climate models, the dynamics of the climate system that determine its response to changes in external forcing.
- **Natural climate variability**, resulting in part from variations in solar and volcanic activity but at least as importantly from the internal dynamics of the climate system, will continue alongside the gradual anthropogenic climate changes.

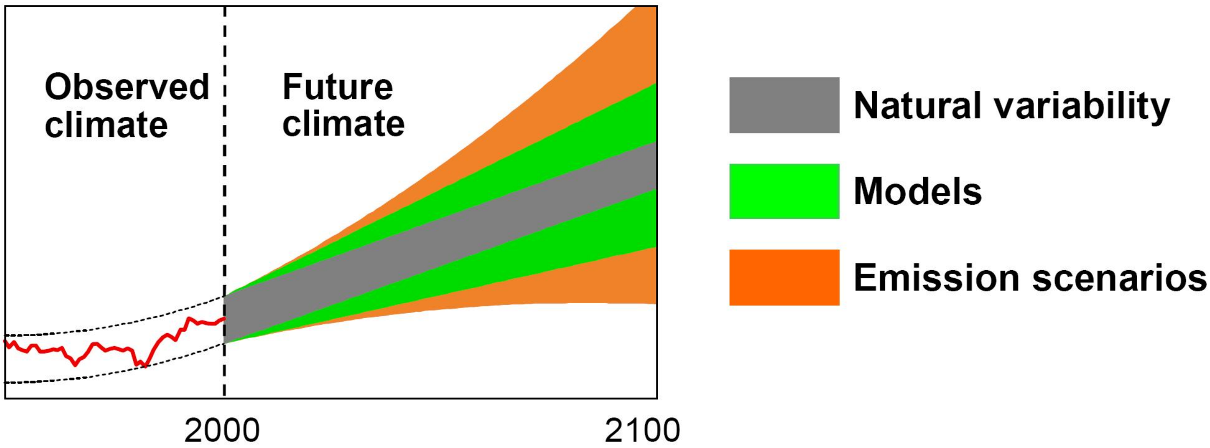

Figure 1.1. *A schematic view of sources of uncertainty in climate change as a function of time (see text for further discussion).*

The relative importance of these uncertainties depends on the time period considered (Figure 1.1). Scenario uncertainty is very important in the long run. For example, the Intergovernmental Panel on Climate Change best estimates for the global mean temperature change by the end of the 21st century vary from 1.8°C to 4.0°C between the SRES scenarios with the smallest (B1) and the largest (A1FI) greenhouse gas emissions (IPCC 2007). For shorter time horizons, however, the scenario uncertainty is much smaller. On one hand, there is inertia in the socio-economical system, and the various scenarios of greenhouse gas emissions therefore still stay relatively close to one another for the next few decades. On the other hand, the atmospheric concentrations of carbon dioxide and other long-lived greenhouse gases react relatively slowly to the changes in emissions.

Modelling uncertainty is in the short run more important than scenario uncertainty, and it also increases with time. The larger the greenhouse gas forcing becomes, the larger absolute effect model errors will have in simulating the response to this forcing. Analogously, the modelling uncertainty is (in the long run) largest for scenarios with large greenhouse gas emissions. Thus, the IPCC (2007) uncertainty range for the 21st century global mean temperature increase for the lowest (B1) emission scenario (1.1-2.9°C) is in absolute terms much narrower than the uncertainty range for the highest (A1FI) scenario (2.4-6.4°C).

Natural variability is generally expected to be the dominating source of uncertainty in short-term climate projections. In high latitudes, in particular, climate is characterized by large interannual and interdecadal variability, which is difficult to predict in any detail even for the near-term future[1]. The uncertainty associated with natural variability does not actually decrease with time: even if there were no other uncertainties, it would still be at least as difficult, and probably more difficult, to forecast the temperatures for the end of this century than for the next decade. However, in comparison with the other, increasing uncertainties, natural variability becomes relatively less important with time.

The depiction of uncertainties in Figure 1.1 is schematic, not quantitative. In addition to the forecast time horizon, the relative importance of the three sources of uncertainty depends on the variable, season and geographical area considered. In particular, natural variability is expected to be relatively more important for local and regional than for global mean climate changes (because, in the global mean, contrasting regional effects of natural variability largely average out). On the other hand, natural variability is expected to be relatively less important for changes in temperature than for changes in many other variables including precipitation, because the greenhouse-gas-induced climate change signal is stronger for temperature than for other variables.

This report presents probabilistic forecasts (or “projections”; these words are used interchangeably here) of temperature and precipitation change for northern Europe in the first

---

[1] Some fraction of natural climate variability might be predictable via a proper initialization of the ocean circulation in climate models (e.g., Keenlyside et al. 2008), or if natural external forcing such as variations in the solar constant could be predicted in advance. However, the research on this subject is still in its infancy, and current understanding suggests that even the potentially predictable fraction of variability in Nordic land areas is modest (e.g., Boer 2000).

half of the 21st century. As such, the report is essentially an update to the report prepared for CES Climate Modelling and Scenarios deliverable D2.2 (Räisänen and Ruosteenoja 2008; hereafter RR08). However, while this previous study was based on results from global climate models (GCMs) alone, we here combine the GCM results with information from higher-resolution regional climate models (RCMs). The present analysis builds on simulations made for the Special Report on Emissions Scenarios (SRES) A1B scenario (Nakićenović and Swart 2000); thus, the emission scenario uncertainty is neglected. However, as suggested by Fig. 1.1 and shown more quantitatively in RR08, this source of uncertainty is secondary when considering climate change in the early 21st century.

Another difference to RR08 is the length of the forecast period. Following the recommendation from the CES all-staff meeting in May 2009, we focus on climate change between the two 30-year periods 1991-2020 and 2021-2050. This will make the uncertainty due to natural variability smaller than it is in forecasts of decadal mean climate change, which were the focus in RR08. This is because natural variations in climate (e.g., cold versus warm or dry versus wet years) tend to average out more completely during a 30-year period than a single decade.

The outline for the rest of this report is as follows. The GCM and RCM simulations used in the analysis are listed in Section 2. Section 3 describes how probabilistic climate change projections are derived by combining the results from the GCM and RCM simulations. In Section 4, the impact of the RCM data on the projections is studied by comparing the GCM plus RCM based projections with those obtained by using GCM data alone. Section 5 presents the GCM plus RCM based projections in more detail, in the form of several maps. This is expected to be the most valuable section for the readers who are more interested in the use of climate scenarios than in the methods used for deriving these scenarios. Finally, the main conclusions are presented in Section 6.

2. Model simulations

We use in our analysis two sets of climate model simulations: GCM simulations from the Third Coupled Model Intercomparison Project, CMIP3 (Meehl et al. 2007), and RCM simulations from the European Union FP6 ENSEMBLES project (Hewitt and Griggs 2004)[2] .

As in RR08, 19 CMIP3 GCMs are used (Table 2.1). The horizontal grid spacing of these models varies from 1.1° latitude × 1.1° longitude to 4° latitude × 5° longitude. For each

[2] Some of the RCM simulations in the ENSEMBLES data base were conducted with funding from other sources, including CES.

model, a 198-year time series (1901-2098) obtained by concatenating the "20th Century Climate in Coupled Climate Models" simulation with the SRES A1B simulation for the 21st century is used. Data from outside the periods 1961-1990 and 2021-2050 are needed by the resampling technique described briefly in Section 3.1 of this report and in more depth by Räisänen and Ruokolainen (2006).

Table 2.1 *The CMIP3 GCMs used in this report.*

Model	Institution
BCCR-BCM2.0	Bjerknes Centre for Climate Research, Norway
CGCM3.1 (T47)	Canadian Centre for Climate Modelling and Analysis
CGCM3.1 (T63)	same as previous
CNRM-CM3	Météo-France
CSIRO-MK3.0	CSIRO Atmospheric Research, Australia
ECHAM5/MPI-OM	Max Planck Institute (MPI) for Meteorology, Germany
ECHO-G	University of Bonn and Model & Data Group, Germany; Korean Meteorological Agency
GFDL-CM2.0	Geophysical Fluid Dynamics Laboratory, USA
GFDL-CM2.1	same as previous
GISS-ER	Goddard Institute for Space Studies, USA
INM-CM3.0	Institute for Numerical Mathematics, Russia
IPSL-CM4	Institut Pierre Simon Laplace, France
MIROC3.2 (hires)	Center for Climate System Research, National Institute for Enviromental Studies and Frontier Research Center for Global Change, Japan
MIROC3.2 (medres)	same as previous
MRI-CGCM2.3.2	Meteorological Research Institute, Japan
NCAR-CCSM3	National Center for Atmospheric Research, USA
NCAR-PCM	same as previous
UKMO-HadCM3	Hadley Centre for Climate Prediction and Research / Met Office, UK
UKMO-HadGEM	same as previous

The 13 RCM simulations used in our analysis are listed in Table 2.2. This set of RCM simulations includes all that were available in the ENSEMBLES Research Theme 3 data base

in mid-June 2009 and (i) had been run at 25 km resolution for the A1B scenario (ii) in a domain considered sufficiently large for our analysis, and (iii) for which no technical problems were detected in an initial inspection of the model output. The data for most of the RCMs were available as interpolated to a regular 0.25° × 0.25° latitude-longitude grid. However, for the present analysis we aggregated the data to a somewhat coarser 0.5° × 0.5° grid. This was done for reducing the computing burden; the loss of information associated with this aggregation is most likely minimal.

Table 2.2 *The RCM simulations used in this report. Institution refers to the institution that conducted the RCM simulation. The model and institution acronyms follow the ENSEMBLES Research Theme 3 web page (http://ensemblesrt3.dmi.dk/)*[3].

Driving GCM	RCM	Institution	Full years
HadCM3Q0	HadRM3Q0	Hadley Centre	1951-2098
	CLM	ETHZ	1951-2098
HadCM3Q3	HadRM3Q3	Hadley Centre	1951-2098
HadCM3Q16	RCA3	C4I	1951-2098
	HadRM3Q16	Hadley Centre	1951-2098
ECHAM5-r3	REMO	MPI	1951-2100
	RACMO2	KNMI	1950-2100
	RegCM	ICTP	1951-2100
	RCA	SMHI	1951-2100
ARPEGE	Aladin	CNRM	1950-2050
	HIRHAM5	DMI	1951-2100
BCM	HIRHAM	METNO	1951-2050
	RCA	SMHI	1961-2099

As indicated by Table 2.2, the RCM simulations are not independent from each other. The 13 simulations are based on horizontal boundary conditions from just six GCMs; for each driving GCM there are regional simulations by one to four RCMs. This is problematic for probabilistic analysis because the RCM solution is strongly affected by the driving GCM simulation. Furthermore, one of the RCMs (RCA-SMHI) has been used in two simulations

[3] HadCM3Q0, HadCM3Q3 and HadCM3Q16 are three versions of the HadCM3 model, differing by the numeric values of some model parameters that impact the simulated climate response to anthropogenic radiative forcing substantially. HadRM3Q0, HadRM3Q3 and HadRM3Q16 are the corresponding versions of the regional HadRM3 model.

with different driving GCMs, and some of the nominally different RCMs are close relatives to each other. As also shown by the table, the length of the RCM simulations varies. For 11 of the 13 RCM simulations, data are available from 1951 (or 1961) to the end of the 21st century, but two of the simulations only extend to the year 2050.

For the sake of simplicity, we assume that all the GCM and all the RCM simulations deserve the same weight in our calculations. This assumption is obviously debatable: for example, one might argue that somewhat lower weight should be given to the four RCM simulations driven by the ECHAM5-r3 GCM simulation, because these RCM simulations are expected to be strongly correlated with each other.

3. Methods used for deriving probabilistic climate change forecasts

The data sets available for the CMIP3 GCMs and the ENSEMBLES RCMs both have their strengths and weaknesses. The global CMIP3 models can be considered as fairly independent from each other, except for some that are relatively close relatives. However, the coarse horizontal resolution of these models compromises their ability to simulate regional variations in climate change, particularly in areas with complex geography. The RCMs have an order of magnitude higher resolution, which allows them to resolve much (although not nearly all) of the regional climatic variability associated with the land-sea distribution and topography. However, the available number of effectively independent RCM simulations is much smaller than the number of GCM simulations.

Consequently, we follow in this study the following principle for deriving probabilistic forecasts of regional climate change:

1. The probability distribution of “large-scale” climate change is estimated from GCM simulations.
2. RCM simulations are used to derive a probabilistic relationship between local and large-scale climate changes.
3. The GCM-based large-scale probability distribution and the RCM-based relationship between local and large-scale climate changes are combined, to obtain probabilistic forecasts of climate change on the local (here: 0.5° lat × 0.5° lon) scale.

The threshold between large and small scale, as required by this method, is not unambiguous. The “large” scale should be so large that the difference between GCM and RCM resolution has no systematic effect on simulated climate change on this scale[4]. On the other hand, the "small" scale should be kept small enough, to prevent the final probability distributions from being dominated too strongly by the RCM data for which the sampling is worse than for the GCM simulations.

In this report, we define "large-scale" climate change as the change in area mean temperature or precipitation over an area of 1500 × 1500 km (see Figure 3.1 – note that the domain is rectangular although it is distorted by the map projection). This large-scale component is defined for each target grid box separately, so that the target location is always in the middle of the large-scale domain. For target locations less than 750 km from the boundaries of the area for which RCM data are available (the grey shading in Figure 3.1), the large-scale domain is reduced in size. For example, for a grid box situated 400 km south of the northern boundary, the large-scale domain is reduced to 800 km in north-south direction, but its width in the east-west direction is kept as 1500 km provided that the eastern and western boundaries are at least 750 km away. Near the corners of the area covered by the RCM data, the large-scale domain is compressed in both the east-west and the north-south directions. As a result, the RCM data have less impact on the final probabilistic forecasts near the borders of the area than in its inner parts.

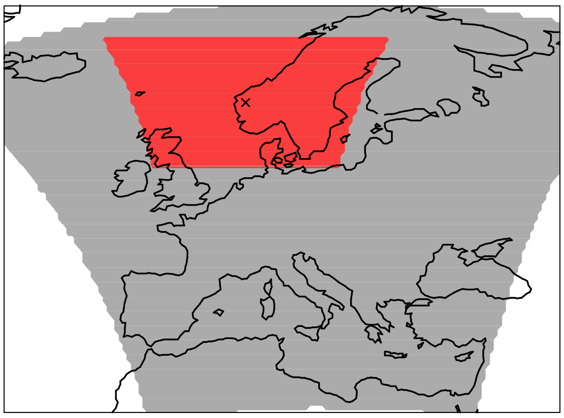

Figure 3.1. *The red shading shows the area used for definition of large-scale climate change, for a target location in western Norway (the cross). The gray shading shows the analysis domain used in this report, defined as the area available for all 13 RCM simulations.*

As an example, Figure 3.2 shows the winter (December-January-February = DJF) mean temperature change from 1961-1990 to 2021-2050 in one of the RCM simulations as divided

[4] In principle, it is possible that this condition is not fulfilled at any scale, because model resolution might have a systematic effect on the simulated climate change that is not averaged out when widening the area (Fronzek and Carter 2007). However, this possibility has not been studied by a systematic comparison between climate changes in RCMs and the driving GCM simulations. In this study as well, such comparison was prevented by the unavailability of most of the GCM simulations used for driving the ENSEMBLES RCMs.

to its large-scale and small-scale (i.e. total – large-scale) parts. As typically turns out to be the case for temperature change, the small-scale component has relatively small amplitude.

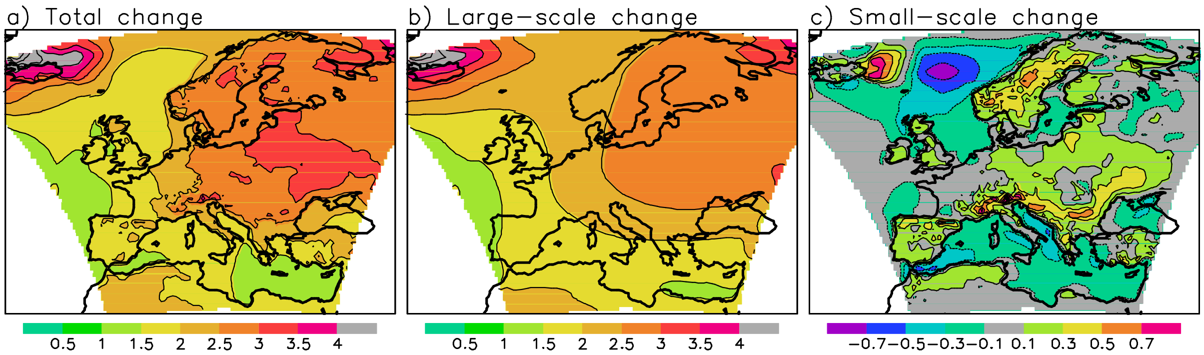

Figure 3.2. *Winter mean temperature change (°C) in the HadRM3Q0/HadCM3Q0 simulation. (a) total change from 1961-1990 to 2021-2050, (b) large-scale change, and (c) small-scale change.*

3.1 Resampling and variance correction

As in RR08, we use here the resampling technique developed by Räisänen and Ruokolainen (2006) for improving the sampling of natural variability. The resampling assumes that the probability distribution of local climate changes is determined by the CMIP3 19-model mean global mean warming; as shown by Räisänen and Ruokolainen (2006), the small systematic biases eventually caused by this approximation are more than compensated by the increase in sample size. Under this assumption, simulated climate changes between any two 30-year periods that share practically the same multi-model global mean temperature change as simulated between 1961-1990 and 2021-2050 (1.35°C) can be taken as plausible realizations of the climate change that could occur between 1961-1990 and 2021-2050. Sub-sampling the latter 30-year period with 5-year interval, 12 such pairs of periods (from 1910-1939 / 2011-2040 to 2021-2050 / 2066-2095) are found for the CMIP3 ensemble, giving a nominal sample size of 19 × 12 = 228.

With the same 5-year sub-sampling interval, 11 suitable pairs of periods are found for those ENSEMBLES simulations that extend from 1951 to the end of the 21st century. For the simulations terminating in 2050, however, the 5-year sub-sampling would only give one valid pair of periods, and even with 1-year sub-sampling only 3 pairs are obtained. Thus, the resampling does not work properly for these models. For simplicity, however, we assume that these simulations deserve the same weight in the calculations as the others. Hence, the few realizations obtained from them are overweighted.

A detail related to resampling is the variance correction described by Ruokolainen and Räisänen (2007). This correction is based on the assumption that an overestimate (underestimate) of interannual climate variability also implies an overestimate (underestimate) of variability on longer time scales. Where the simulated interannual variability in a given model exceeds (is smaller than) the observed variability, there the variance of the resampled realizations is artificially reduced (amplified) to compensate for this bias. Here we only apply the variance correction to the large-scale climate changes inferred from the CMIP3 ensemble, not to the data from the ENSEMBLES RCM simulations (the latter would be complicated because of the way in which these data are used).

The internannual variances required by the variance correction were calculated from detrended 20th century (1901-2000) time series of simulated temperature and precipitation, and from observations from the University of East Anglia Climate Research Unit (CRU) TS 2.0 data set (Mitchell et al. 2004). Because the CRU data only cover land areas, the large-scale area means of temperature and precipitation were simply calculated as area means over those grid boxes within the 1500 × 1500 km domain for which data were available (and excluding such isolated island grid boxes where the variability in the CRU data set is unrealistically low). The same masking was applied when calculating the internannual variance of large-scale climate in the CMIP3 simulations. The ratio between the simulated and observed variances obtained in this way was also assumed to be valid for full 1500 × 1500 km area means. Obviously, the reliability of this procedure is questionable over the Atlantic Ocean, where the large-scale area means cannot be well approximated by the available land- and island-based observations.

As shown by Ruokolainen and Räisänen (2007), the variance correction has a slight tendency to increase the spread of precipitation change projections in northern Europe, because the simulated interannual precipitation variability in the CMIP3 models is typically somewhat lower than observed. Its effect on temperature change projections is rather modest.

3.2 Relationship between local and large-scale climate changes in ENSEMBLES simulations

Figure 3.3 shows the relationship between large-scale and local winter mean temperature and precipitation changes, as diagnosed from the resampled ENSEMBLES ensemble, in a grid box in western Norway. As expected, the local changes tend to increase with the large-scale changes. However, as generally turns out to be the case, this relationship is much tighter for temperature (the large-scale change explains 86% of the variance of the local change) than for precipitation (only 40% of the variance of the local change is explained[5]).

[5] These numbers give the explained variance as calculated directly from the data set. They give an upward biased estimate of the fraction of explained variance in the population from which the data come from.

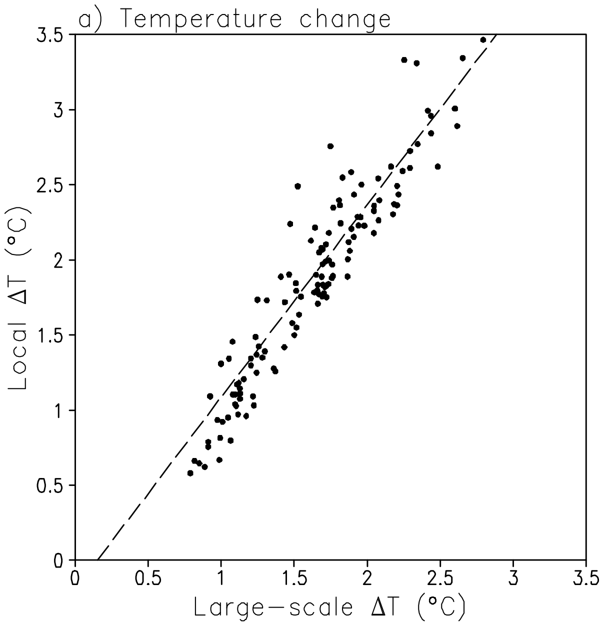

Figure 3.3. *Analysis of winter mean climate changes in the resampled ENSEMBLES RCM simulations, in a grid box in western Norway (61.25°N, 6.25°E). In (a), the horizontal axis shows the area mean temperature change for a 1500 × 1500 km square centred at this location (shown in Fig. 3.1), the vertical axis the local temperature change. The dashed line is the linear regression line of Eq. (3.1). (b) As (a), but for precipitation changes.*

In the location of Fig. 3.3, the best-fit linear regression lines that link the local temperature and precipitation changes to the large-scale change have slopes exceeding one (1.3 for temperature, and 2.0 for precipitation). For temperature change, a slope coefficient exceeding unity is unsurprising because, in this case, the large-scale area includes a substantial fraction of ocean (see Fig. 3.1) and land is generally expected to warm faster than sea. The very high coefficient for precipitation turns out to be unusual, but it can also be explained by the geographic location of the grid box chosen for this example. We speculate that the physical explanation is as follows:

- On both the local and larger scales, changes in winter precipitation result mainly from a combination of two factors: (i) an increase in northward and ocean-to-land water vapour transport resulting from the larger moisture content of a warmer atmosphere, and (ii) changes in atmospheric circulation. The former factor is expected to be quite robust, but the latter is more variable among model simulations and also sensitive to natural variability.
- An increase in westerlies would induce a substantial increase in local orographic precipitation on the western slopes of the Scandinavian mountains. It would also enhance the increase in large-scale precipitation (partly because of increased eastward moisture advection from the Atlatnic Ocean, partly because an increase in westerlies

implies a northward shift in cyclone activity), but this large-scale effect should not be as strong.

- Thus, the strong increase in local precipitation with increasing large-scale precipitation in Fig. 3.3b likely reflects the fact that the precipitation in this particular location is more sensitive to atmospheric circulation than the large-scale precipitation in the surrounding area.
- The regression line in Fig. 3.3b also indicates that, for a zero large-scale precipitation change, the local precipitation in western Norway would decrease. This is physically plausible. For the large-scale precipitation not to increase, the increased water vapour transport resulting directly from the warming of the atmosphere should be compensated by a southward shift in cyclone activity and weakened time-mean westerlies. Given that the local precipitation in western Norway is relatively more sensitive to the atmospheric circulation than the large-scale precipitation is, the local precipitation would decrease in such a situation.

To link the local temperature and precipitation changes (Δx_{Loc}) to the corresponding large-scale climate changes (Δx_{Large}), we apply ordinary linear regression to the resampled ENSEMBLES data:

$$\Delta x_{LOC} = a \Delta x_{LARGE} + b + e \tag{3.1}$$

Here, a is the slope coefficient and b a constant offset, whereas e represents a stochastic residual not explained by the large-scale climate change. We assume e to be normally distributed with zero mean and variance

$$\varepsilon^2 = \frac{1}{N} \sum_{i=1}^{N} (\Delta x_{LOC} - a \Delta x_{LARGE} - b)^2 \tag{3.2}$$

By neglecting the sampling uncertainty in a and b, (3.2) gives a downward biased estimate of the residual variance. However, this bias is not easily corrected for the resampled ENSEMBLES data set in which the different realizations of climate change are not independent.

The first four rows of Figs. 3.4 and 3.5 show the diagnosed geographical distributions of a, b, and ε for temperature and precipitation change in the four three month-seasons (DJF = December-January-February, MAM = March-April-May, JJA = June-July-August, SON = September-October-November) and for the annual mean. In the last row of the figures, the fraction of variance explained by the regression is shown. This, together with ε, shows how tightly local climate changes are controlled by the large-scale climate change within the ENSEMBLES data set.

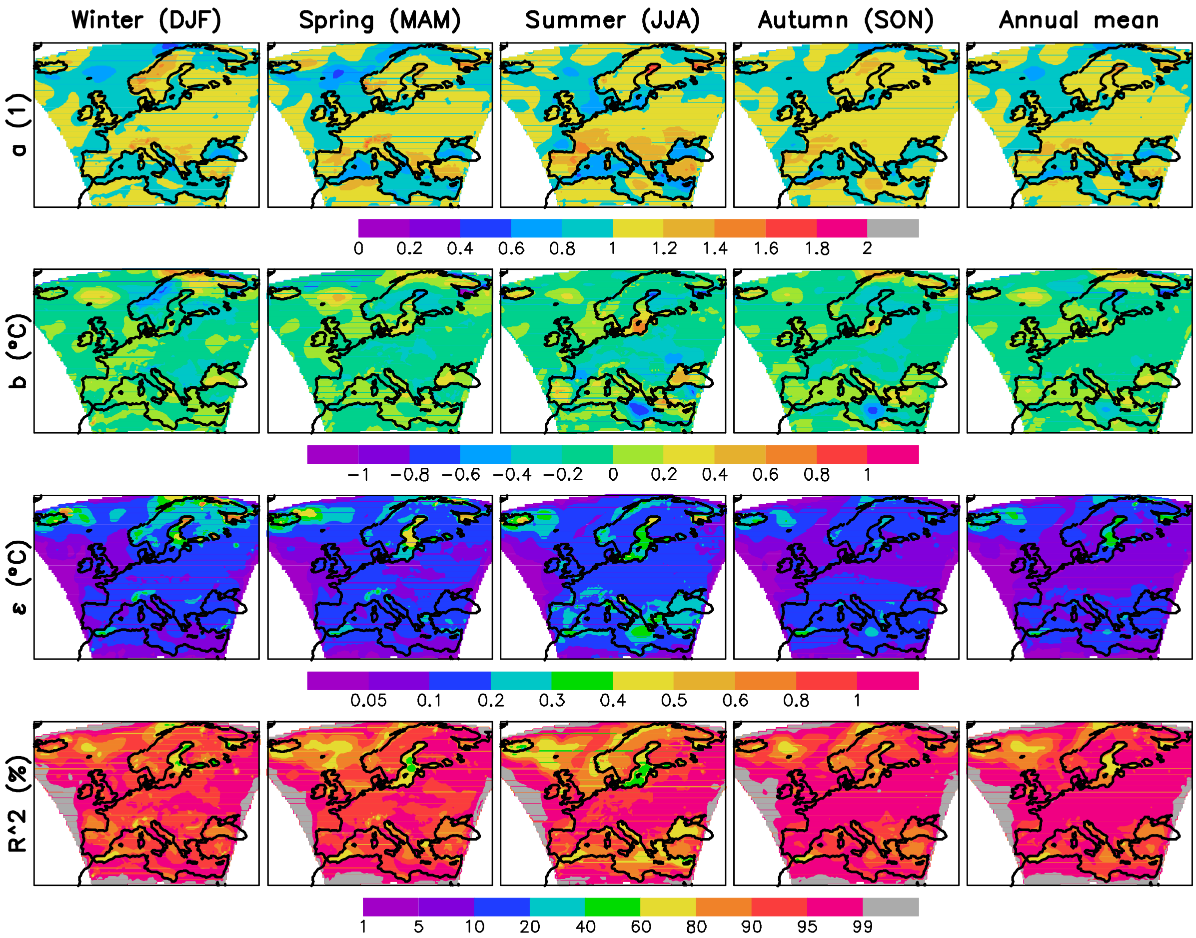

Figure 3.4. *Relationship between local and large-scale temperature changes in the resampled ENSEMBLES RCM simulations. The first row shows the slope coefficient in (3.1), the second the constant offset, the third the square root of the residual variance and the fourth the fraction of variance explained by the linear regression.*

As expected, the slope coefficients vary on both sides of unity[6]. For changes in temperature (Figure 3.4), the variation is relatively small, but the tendency to larger warming (and larger circulation-sensitivity of the warming) over land than sea is reflected as coefficients exceeding one over most land areas. The effects of orography can also be seen, most clearly over the Alps in spring. A maximum in slope also occurs over the Bothnian Bay in summer; however, in this area the regression residuals are also large. In the case of precipitation (Figure 3.5), the slope coefficients are much more variable. A distinct maximum with $a \approx 2$ occurs along the western coast of Norway in winter and to a lesser extent in autumn. The constant offsets b show some tendency to anticorrelation with a, particularly for temperature

[6] A slight systematic tendency for the coefficients to exceed one can be seen, particularly for precipitation. This can be explained by the fact that the large-scale domain is always centred at the target grid box. To understand this, assume that the large-scale domain were fixed in location. In this case, the mean of the slope coefficients over its area would be exactly one (at least for temperature, for which the change is given in absolute units). However, coefficients exceeding unity would be more common in the middle of the domain, where the local climate change is typically best correlated with the large-scale change.

but to some extent also for precipitation. This might partly be an artefact of sampling variability; however, as discussed above for the grid box in western Norway, physical explanations are also plausible.

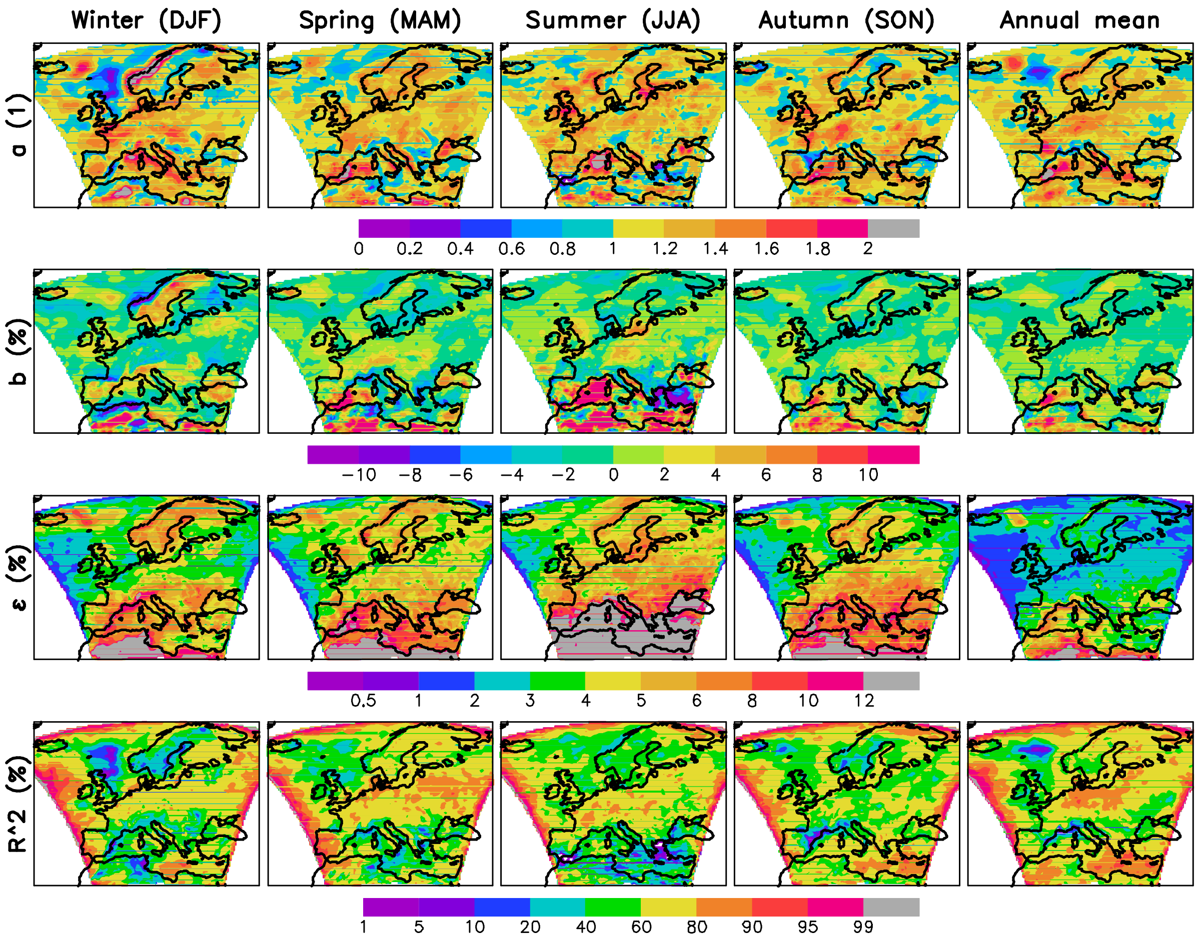

Figure 3.5. *As Figure 3.4, but for precipitation changes.*

Changes in local temperature are strongly controlled by the large-scale temperature change. This is reflected both by the small amplitude of the regression residuals (typically 0.1-0.3°C) and the large explained variance (mostly above 80%, with some exceptions like the Baltic Sea). For changes in precipitation, the correlation between the local and the large-scale changes and hence the explained variance is lower. The explained variance varies on both sides of 60% for seasonal precipitation changes, and is only slightly higher for annual mean precipitation change. Also note that the explained variance typically increases, and the residuals decrease, towards the boundaries of the domain. This is caused by the decrease in the area used for defining "large-scale" climate changes near the borders of the RCM domain.

To derive our probabilistic forecasts of temperature and precipitation change, we use the regression coefficients (*a*, *b* and ε) diagnosed from the ENSEMBLES data set to convert the 228 realizations of large-scale climate change from the resampled CMIP3 ensemble to plausible realizations of local climate change. The stochastic residuals *e* are added as normally distributed random numbers (10 per each CMIP3 realization of large-scale climate change).

This procedure is illustrated in Fig. 3.6. The first panel shows winter mean temperature and precipitation changes for the 1500 km × 1500 km area surrounding the grid box used in Fig. 3.3, as obtained from the resampled CMIP3 ensemble. In the second panel, the CMIP3 simulated large-scale changes are transformed using (3.1), but excluding the stochastic residuals *e*. Because, the slope coefficients of both temperature and precipitation change exceed one in this grid box, the distributions of both temperature and precipitation change grow wider (but the widening is larger for precipitation change). The distributions are additionally widened when the stochastic residuals are added as random numbers (the last panel). The tendency of the realizations of temperature and precipitation change to fall on straight lines in Fig. 3.6c is artificial – this is due to the fact that the same sequence of random numbers is used for both variables. As implemented here, the method does not take into account the correlation of temperature and precipitation change residuals, although this could be done in principle, if joint distributions of temperature and precipitation change were needed.

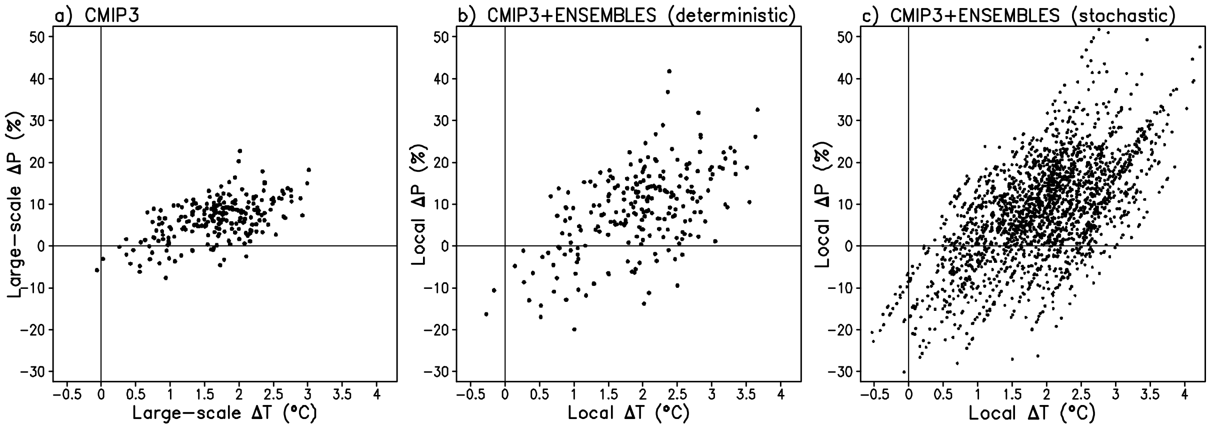

Figure 3.6. *Realizations of winter mean temperature (horizontal axis) and precipitation change (vertical axis). (a) Area mean changes over the 1500 km × 1500 km area surrounding the grid box (61.25°N, 6.25°E) in the resampled CMIP3 ensemble. (b) Transformation of the large-scale temperature and precipitation changes to local changes using (3.1) but excluding the stochastic residuals. (c) as (b) but including the stochastic residuals. The tendency of temperature and precipitation changes to fall on straight lines in (c) is artificial (see text).*

3.3 Comparison of large-scale climate changes between the CMIP3 and ENSEMBLES simulations

If the statistical distribution of large-scale climate changes agrees between the RCM and the GCM ensembles, then our method will return a distribution similar to that obtained directly from the RCM simulations. On the other hand, if the differences in large-scale climate change between the two data sets were very large, this might deteriorate the reliability of our method as the regression relationship (3.1) would need to be extrapolated far beyond the range that it was derived for.

In fact the differences between the CMIP3 and ENSEMBLES data sets are quite small, at least as far as the mean of large-scale climate changes is considered. The annual mean temperature changes differ mostly less than 0.1°C (Figs. 3.7a-c) and the changes in annual precipitation typically by about one percent (Figs. 3.8a-c). Slightly larger, but still modest differences occur in seasonal mean climate changes (Figs. 3.9-3.10, top). For example, the average winter mean warming in eastern Finland and northern Russia is about 0.5°C smaller in the ENSEMBLES than in the CMIP3 data set.

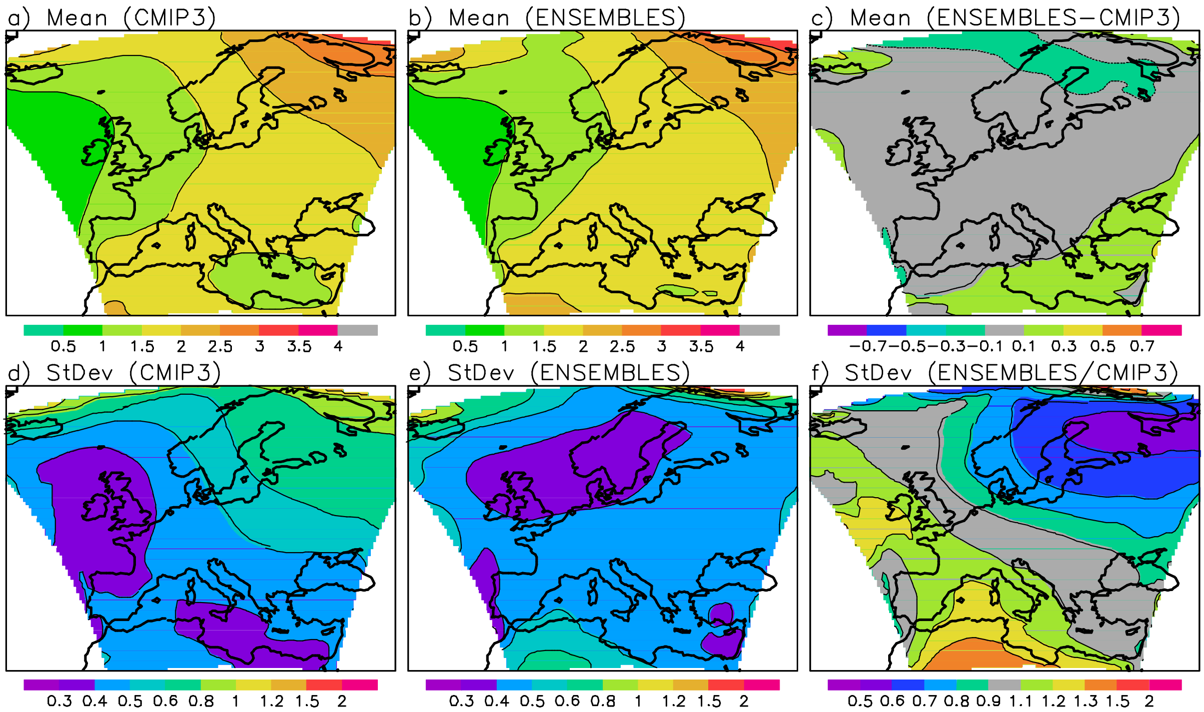

Figure 3.7. *Comparison of large-scale annual mean temperature changes (°C) within the resampled CMIP3 and ENSEMBLES data sets. Top: mean changes and their difference. Bottom: standard deviations and their ratio.*

There are more marked differences between the spread of the two ensembles. Large-scale temperature changes in northern Europe vary less within the ENSEMBLES than within the CMIP3 data set. This is the case for both the annual mean temperature change (Fig. 3.7, bottom) and for the changes in the individual seasons (Fig. 3.9, bottom). The conclusions for precipitation are less clear-cut. The standard deviation of large-scale annual mean precipitation change over Scandinavia is slightly larger in the ENSEMBLES than in the CMIP3 ensemble (Fig. 3.8, bottom). In winter, however, large-scale precipitation changes over the Nordic area are less variable (by 10-50% in standard deviation) in the ENSEMBLES than in the CMIP3 data set (Fig. 3.10, bottom).

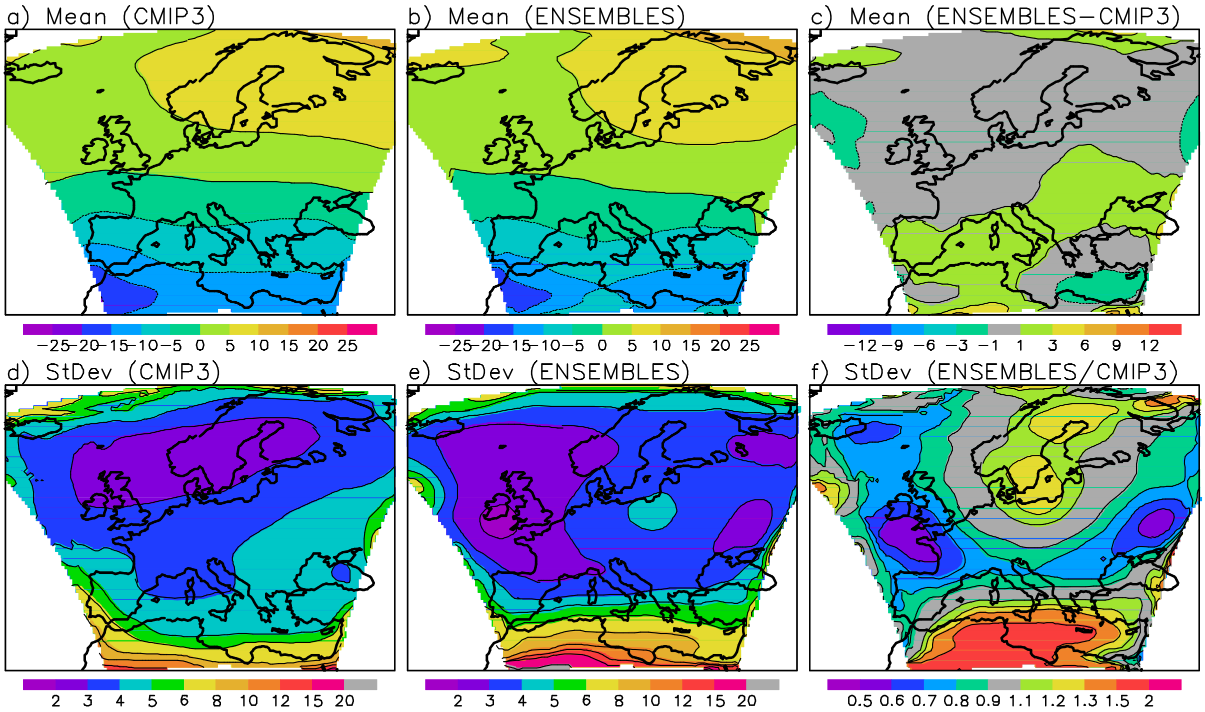

Figure 3.8. *Comparison of large-scale annual mean precipitation changes (%) within the resampled CMIP3 and ENSEMBLES data sets. Top: mean changes and their difference. Bottom: standard deviations and their ratio.*

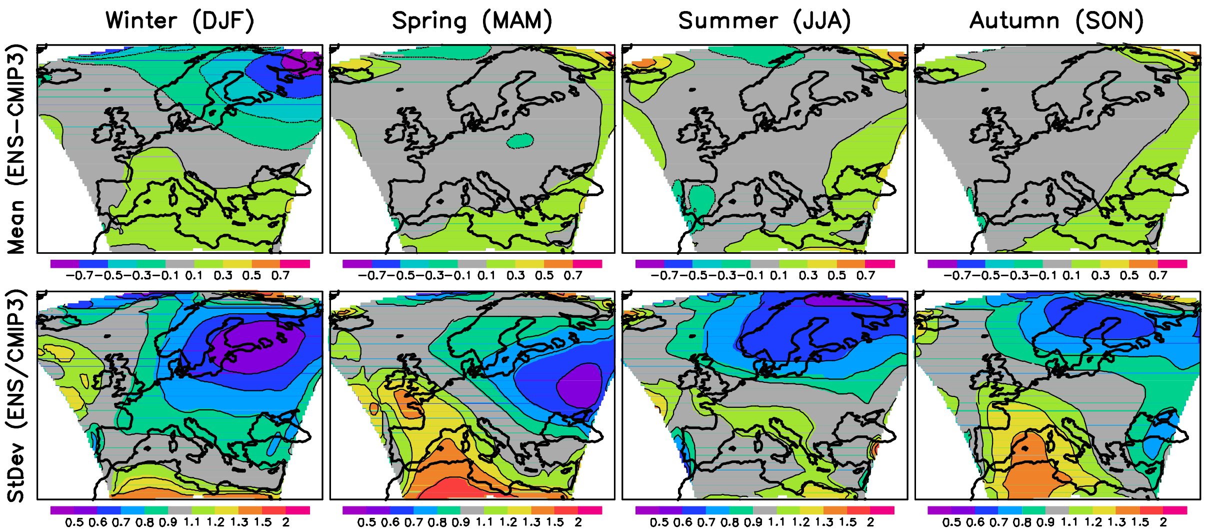

Figure 3.9. *Comparison of large-scale seasonal mean temperature changes between the resampled CMIP3 and ENSEMBLES data sets. Top: ensemble mean difference ENSEMBLES – CMIP3 (°C). Bottom: ratio between the standard deviations in the ENSEMBLES and the CMIP3 data sets.*

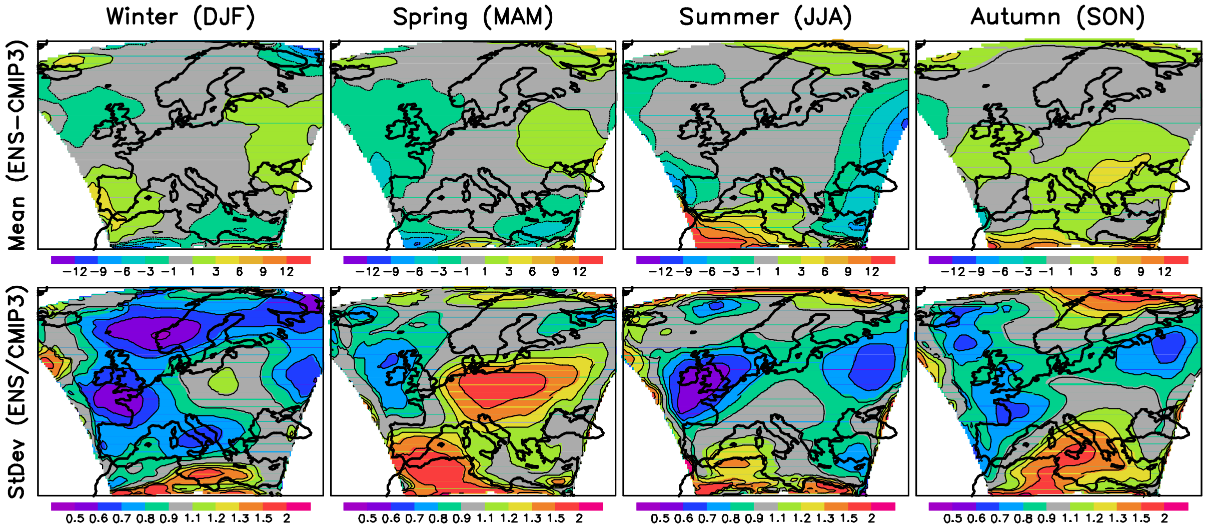

Figure 3.10. *Comparison of large-scale seasonal mean precipitation changes between the resampled CMIP3 and ENSEMBLES data sets. Top: ensemble mean difference ENSEMBLES – CMIP3 (%). Bottom: ratio between the standard deviations in the ENSEMBLES and the CMIP3 data sets.*

4. Impact of RCM data on forecasts of climate change

In RR08, probabilistic forecasts of climate change were derived using the CMIP3 ensemble of GCM simulations. In this section, the impact of adding RCM information is studied. Here, we simply characterize the forecasts by their mean and standard deviation; other characteristics of the probability distributions will be studied in the next section.

The discussion in Section 3 suggests at least three ways of deriving forecasts of climate change: (i) from GCM simulations alone, (ii) from RCM simulations alone, and (iii) by combining the GCM- and the RCM-based information. Figures 4.1-4.4 compare these alternatives with each other, with a fourth column included for the difference of (iii) and (i) to illustrate the impact of the RCM data in the last method.

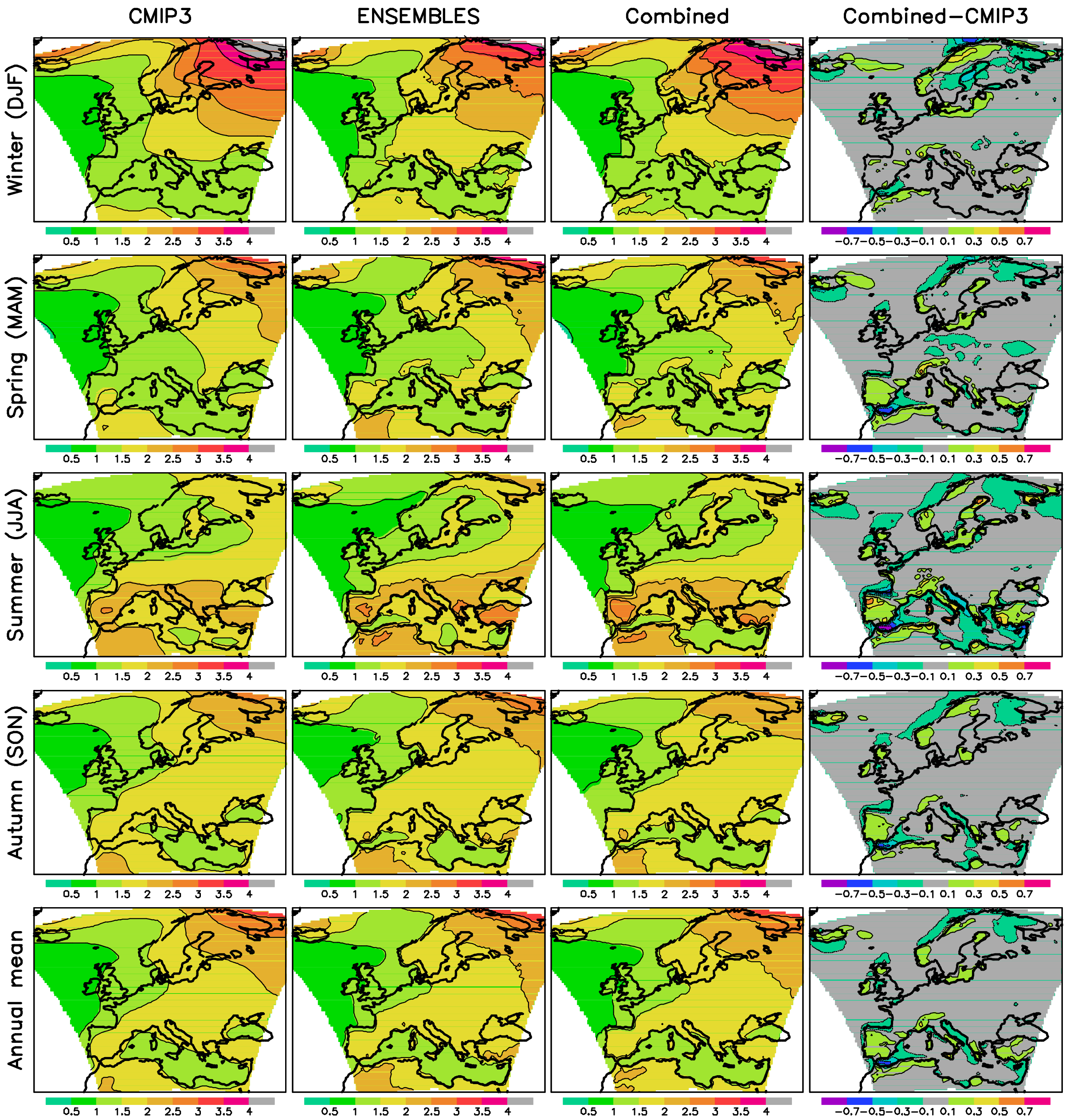

Figure 4.1. *Ensemble mean seasonal and annual mean temperature changes (°C) for the resampled CMIP3 GCM simulations and ENSEMBLES RCM simulations (first and second columns), and for the combination of the two data sets (third column). The last column shows the difference between the third and the first columns. The changes represent the mean temperature difference between 2021-2050 and 1961-1990.*

An inspection of the ensemble mean temperature changes (Fig. 4.1) reveals a remarkable similarity between the three methods. However, the ENSEMBLES simulations show sharper gradients along the coastlines than the lower-resolution CMIP3 simulations. The combination of the CMIP3 and ENSEMBLES data (third column) retains the small-scale patterns from the ENSEMBLES simulations. However, where larger-scale differences between CMIP3 and ENSEMBLES exist, such as in the northeastern corner of the domain in winter, the absolute magnitude of the warming in the combined CMIP3 plus ENSEMBLES projection is closer to that in the CMIP3 ensemble. Consequently, the impact of the RCM data on the mean of the temperature change projections is modest in absolute terms, almost invariably less than 0.3°C (fourth column). The most notable features in the Nordic area include a slight increase in warming in western Norway, and a slight decrease in warming in northeastern Fennoscandia.

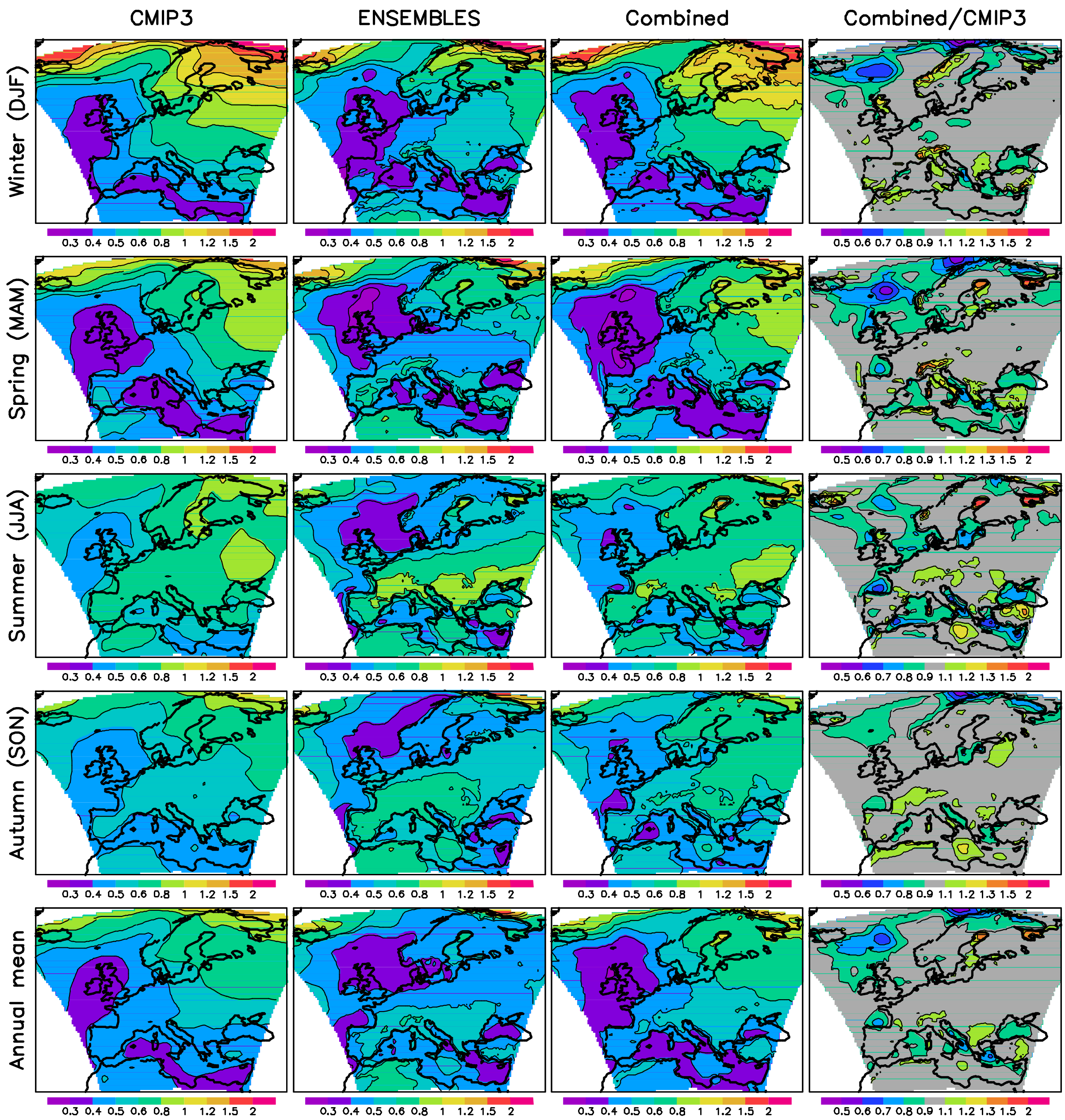

Figure 4.2. *As Figure 4.1, but for the standard deviation of temperature change (unit: °C). The last column shows the ratio between the standard deviations in the third and the first columns.*

A comparison between the first two columns in Fig. 4.2 shows that the standard deviation of temperature changes in northeastern Europe is mostly smaller in the ENSEMBLES than in the CMIP3 ensemble; in southwestern Europe, the difference is reversed. Nevertheless, the combination of the CMIP3 and ENSEMBLES ensembles yields standard deviations that are mostly within 10% from those obtained directly from CMIP3. One exception is western

Norway, where the standard deviation of winter mean temperature change is amplified locally by about 30%. The comparison also reveals some “hot spots” over regional-scale water bodies, such as the Bothnian Bay and the White Sea, where temperature changes are more variable in the ENSEMBLES data set and in the combined CMIP3 plus ENSEMBLES ensemble than among the CMIP3 simulations. These hot spots are most pronounced in summer.

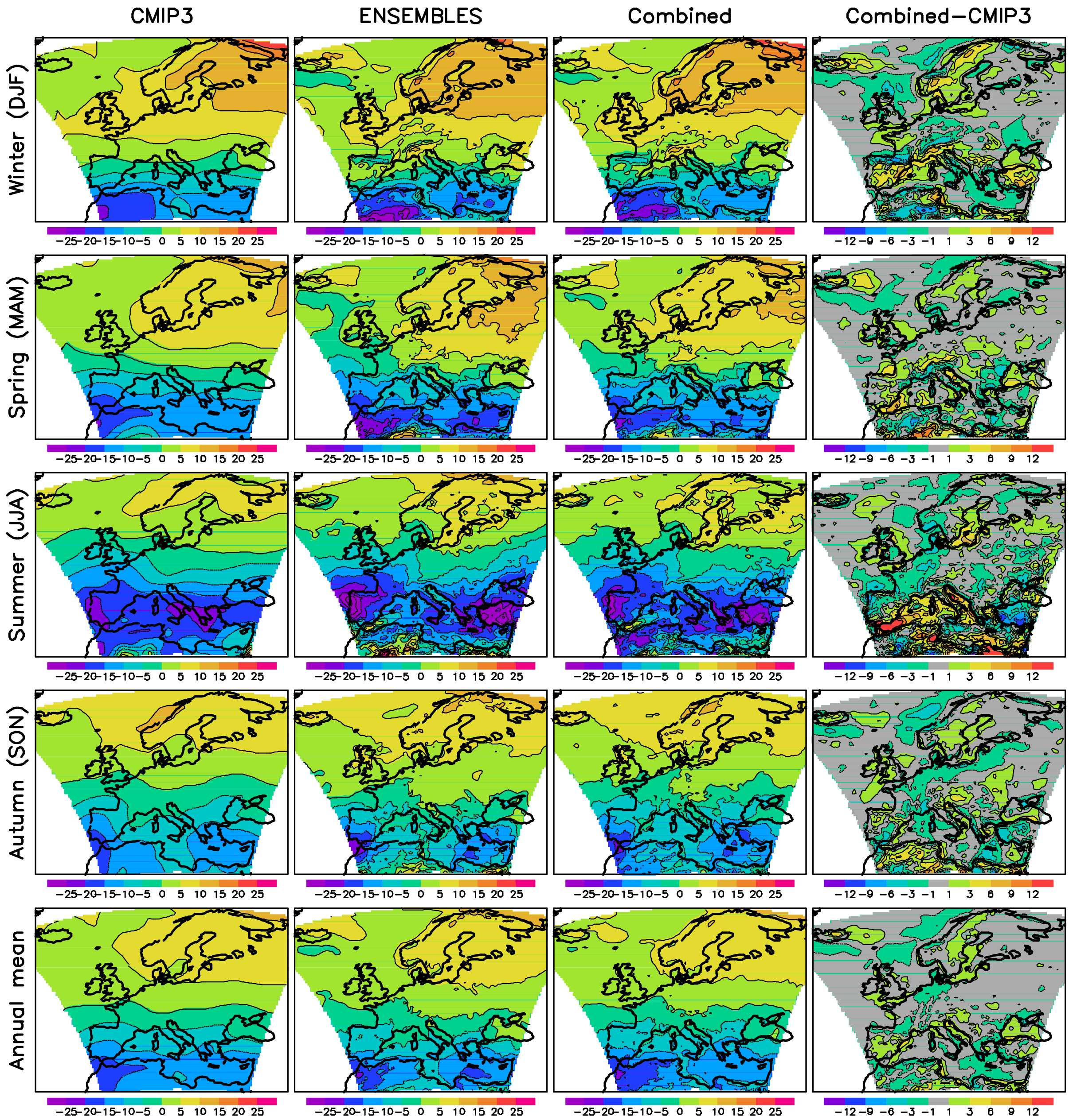

Figure 4.3. *Ensemble mean seasonal and annual mean precipitation changes for the resampled CMIP3 GCM and ENSEMBLES RCM simulations (first and second columns), and for the combination of the two data sets (third column). The last column shows the difference between the third and the first columns. The changes represent the per cent difference in mean precipitation between 2021-2050 and 1961-1990.*

Ensemble means of precipitation change are also similar between CMIP3, ENSEMBLES and their combination (Figure 4.3). Most notably, the differences in annual mean precipitation change between the combined data set and the CMIP3 ensemble (bottom right panel) are typically of the order of only one percent. Somewhat larger differences are apparent on the seasonal time scale. For example, the ensemble mean of the ENSEMBLES simulations and the combined ensemble both suggest a relatively sharp gradient in winter precipitation change across Scandinavia, with a larger per cent increase on the eastern than the western side of the Scandinavian mountains. A similar feature is seen in the CMIP3 results, but the gradient is much smoother. However, as can be seen from Figure 4.4, changes in winter precipitation in western Norway have a rather large uncertainty.

The standard deviation of precipitation change (Figure 4.4) shows few systematic differences between the three ensembles, but there are some differences in the seasonal and regional details. A striking feature in the combined CMIP3 plus ENSEMBLES ensemble is the local maximum in the standard deviation of winter precipitation at the west coast of Norway, which is not resolved by the lower-resolution CMIP3 ensemble. This reflects in part the large variability of winter precipitation changes in this area in the ENSEMBLES simulations, which most likely results from the strong circulation sensitivity of precipitation caused by the local geography. However, the standard deviation in the combined data set actually exceeds that obtained directly from the ENSEMBLES data. This is because the large-scale winter mean precipitation in this area is more variable within the CMIP3 than the ENSEMBLES data set (Figure 3.10).

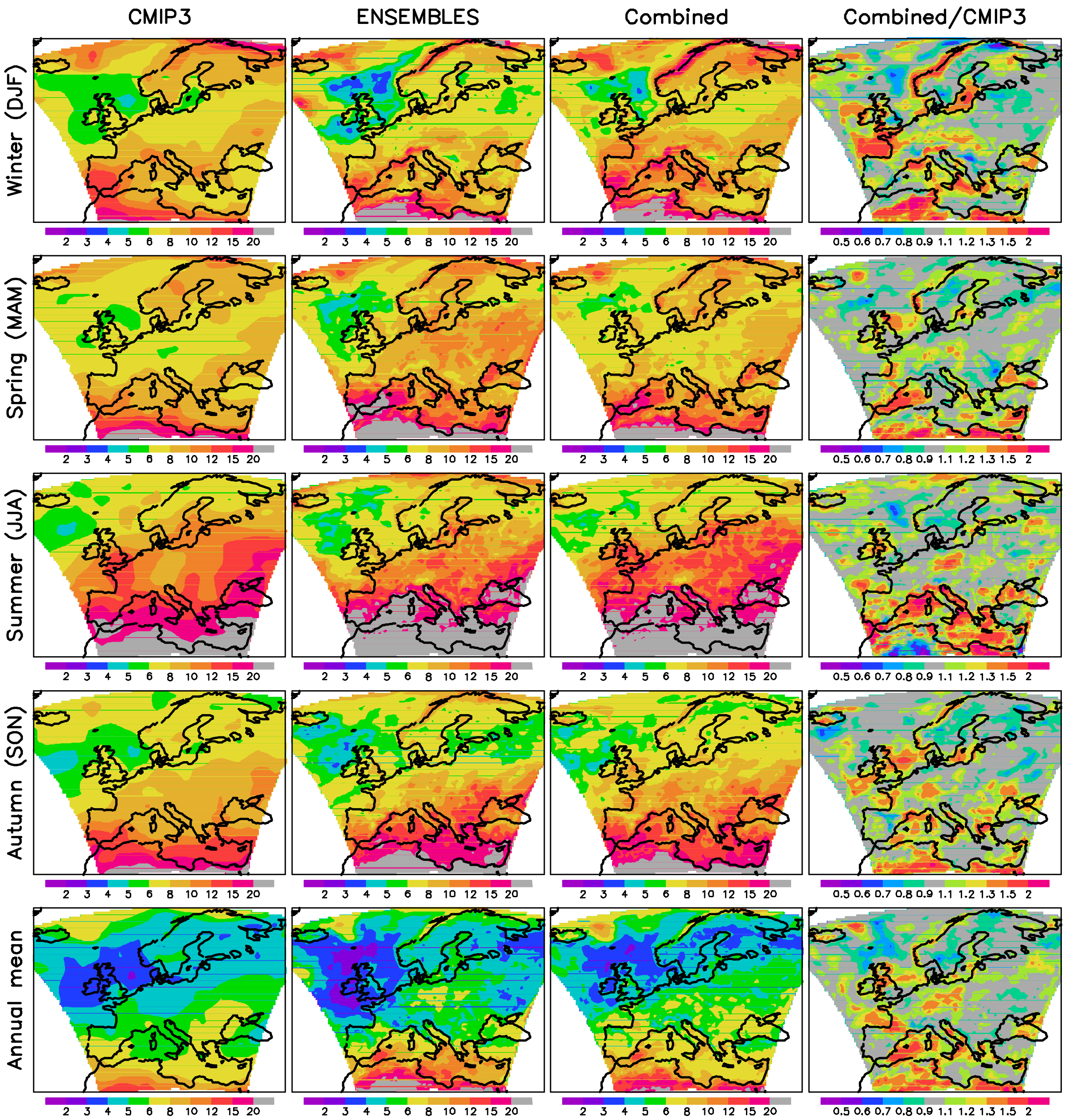

Figure 4.4. *As Figure 4.3, but for the standard deviation of precipitation change (in per cent of the mean precipitation in 1961-1990). The last column shows the ratio between the standard deviations in the third and the first columns.*

In summary, the higher resolution of the RCM simulations has a relatively modest effect on the resulting climate change projections. The conclusions from the earlier GCM based analysis by RR08 remain therefore largely valid. Nevertheless, the RCM data do add some physically plausible small-scale detail in the projections. Land-sea contrasts in temperature change near coastlines are more sharply resolved, as is the impact of orography on precipitation changes. However, the RCMs do not eliminate the uncertainty in the forecasts. The uncertainty estimates obtained by combining the information from the CMIP3 and ENSEMBLES simulations are generally similar to those obtained directly from the CMIP3 data set. In some specific cases, such as for the change in winter precipitation in western

Norway, the higher-resolution data in fact reveal a larger uncertainty than was visible from the coarser-resolution CMIP3 results.

5. Probabilistic projections of temperature and precipitation change

In this section, probabilistic projections of temperature and precipitation change are presented. As noted earlier in this report, there are three main differences between these projections and the ones given in RR08:

1. Following the recommendation from the CES annual meeting in May 2009, the baseline period has been shifted from 1971-2000 to 1961-1990. This backward shift in baseline acts to make the simulated climate change between the baseline and any future period slightly larger.
2. A 30-year forecast period (2021-2050) is considered instead of individual decades. Because 30-year means in temperature and precipitation are affected less by natural variability than decadal means, this change acts to narrow the uncertainty range in the projections.
3. Results from the global climate models (GCMs) used in RR08 are combined with higher-resolution (25 km) regional climate model (RCM) simulations from the ENSEMBLES project, using the methods described in Section 3. As discussed in Section 4, this change has a relatively small impact on the projections, although it adds physically credible small-scale detail particularly near coastlines and mountain ranges.

5.1 Best estimates and uncertainty ranges of temperature and precipitation change

Figure 5.1 depicts the 5th, 50th and 95th percentiles of the calculated probability distribution of temperature change. As far as the method of estimating the probabilities is valid, there is by definition a 90% probability that the changes in the real world will fall between the 5th and 95th percentiles. The 50th percentile (i.e., the median) represents the best estimate of the change.

As the best estimate, an annual mean warming of about 1.5°C is projected for Iceland, Denmark and the west coast of Norway. Elsewhere in the Nordic area, the warming is slightly larger, approaching 2.5°C in northernmost Finland and northern Russia. The largest warming is projected in winter and the smallest in summer. This seasonal contrast is strongest in the northeastern parts of the Nordic area. Further south, in the Mediterranean area, the seasonal cycle of the warming is reversed. Except for the absolute magnitude of the change, which is affected by the choice of the baseline and forecast periods, these general features are very similar to those reported in RR08. However, the land-sea contrast in warming in coastal areas is resolved more sharply by the higher-resolution RCM simulations.

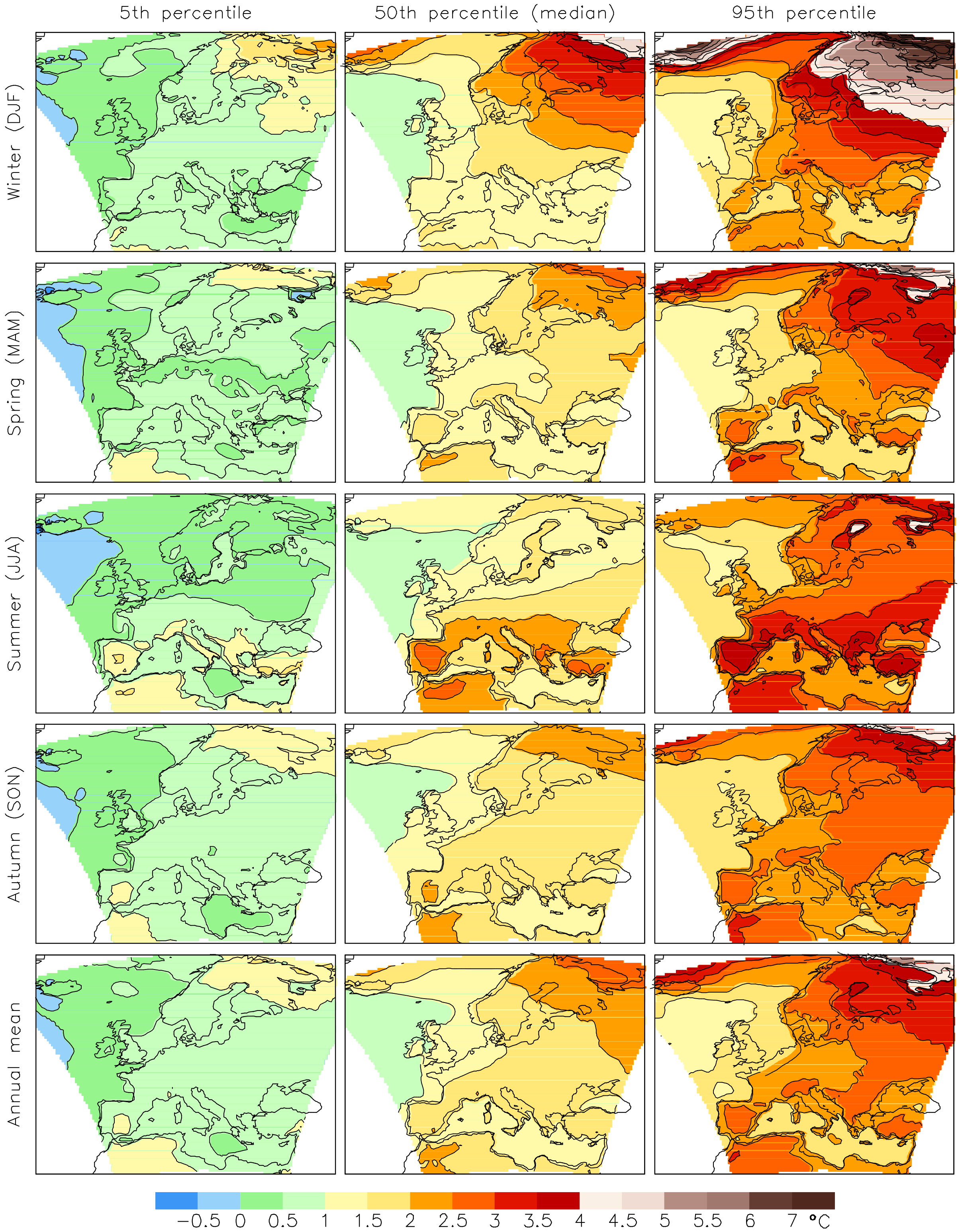

Figure 5.1. *The 5th, 50th (median) and 95th percentiles of the probability distribution of temperature change. The changes represent 30-year seasonal and annual mean temperature differences between the periods 1961-1990 and 2021-2050. The colour scale is given below the figure.*

The uncertainty range in the temperature projections is non-negligible: the 5th percentile is generally less than half of the best estimate warming, whereas the 95th percentile is at least 50% above the best estimate. The 5th percentile of the annual mean change ranges from near zero in Iceland to slightly over 1°C in northern parts of Finland and Scandinavia, the 95th percentile from slightly over 2°C at the south coast of Iceland and west coast of Norway to 3.5°C in northern Finland. The uncertainty in seasonal mean temperature changes is larger, particularly in winter when the 95th percentile of the warming exceeds 5°C in the northeastern parts of Fennoscandia. The maps for the 95th percentile also indicate a possibility of rather large warming (up to over 4°C) over the Bothnian Bay and the White Sea in summer. This feature is difficult to interpret because it might be associated with the simple treatmetnt of these water bodies in the ENSEMBLES simulations.

The corresponding 5th, 50th and 95th percentiles of precipitation change are shown in Fig. 5.2. As the best estimate, the models suggest an annual mean precipitation increase of 5-10% over most of northern Europe. The change is generally largest in winter, when it exceeds 10% in southeastern Norway, Sweden, Finland and northern Russia. The best-estimate precipitation change in summer is marginally negative in Denmark, the west coast of southern Sweden and southernmost Norway, but positive further north and east in Fennoscandia. In Iceland, there is little seasonal cycle in the change, with a weak maximum in autumn.

A regional feature that was not resolved in the GCM-based analysis of RR08 is a contrast in the change in winter precipitation across the Scandinavian mountains, with larger increases over the southeastern than the northwestern slopes of the mountain range. However, this pattern is not completely robust: an inspection of the ENSEMBLES data set reveals that the opposite pattern with larger precipitation increases at the west coast of Norway than further inland actually occurs in a few of the RCM simulations (not shown).

Changes in precipitation are in relative terms more uncertain than the changes in temperature. The 5th percentile of annual mean precipitation change is positive in northern Russia, Finland and large parts of Sweden; elsewhere, it is generally negative. Conversely, the 95th percentile is in the range 10-20%. The uncertainty in seasonal mean precipitation changes is larger than that of the annual mean change. In particular, the 5-95% range of wintertime precipitation change in western Norway extends from a 20% decrease to a 35% increase. This likely reflects the high sensitivity of winter precipitation in western Norway to variations in the atmospheric circulation – much more snow and rain falls with westerly than with easterly winds – together with the variation of circulation changes among climate model simulations (see Räisänen et al. 2004).

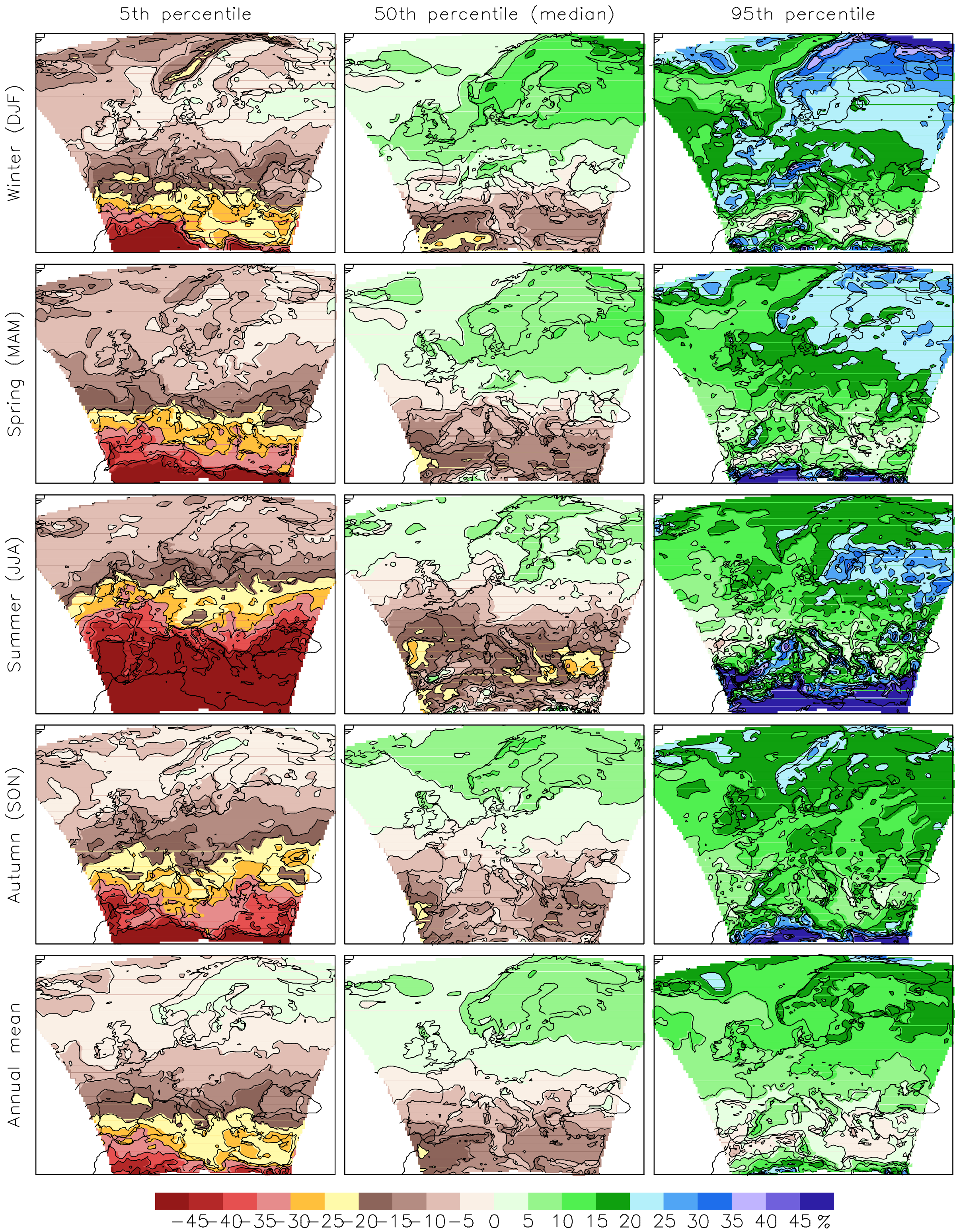

Figure 5.2. *The 5th, 50th (median) and 95th percentiles of the probability distribution of precipitation change. The changes represent 30-year seasonal and annual mean precipitation differences between the periods 1961-1990 and 2021-2050 and are given in per cent of the mean precipitation in the former period. The colour scale is given below the figure.*

5.2 How probably will temperature increase (precipitation change) by at least X°C (Y%)?

Another useful tool for illustrating the results of probabilistic analysis are maps of exceedance probability. Such maps show the probability of observing a climate change of at least given magnitude, e.g., a warming of 1°C or more. Figures 5.3-5.4 show such maps for six thresholds of temperature change, from zero to 5°C. For precipitation, probability maps are given both for increases ranging from zero to 25% (Figs. 5.5-5.6) and for decreases of up to 10% (Fig. 5.7).

The contents of these maps are consistent with the percentile analysis in Figs. 5.1-5.2. Therefore, it is unnecessary to discuss them in all detail. Rather, we only point out a few interesting features:

- The probability that the climate in 2021-2050 will be at least slightly warmer than it was in 1961-1990 is very high, generally exceeding 98% (the maps for $\Delta T > 0$ in Fig. 5.3). As far as the annual mean temperature change is concerned, this is the case even in Iceland, despite a slight chance of cooling over the northern North Atlantic.
- When increasing the threshold of warming, the exceedance probabilities naturally decrease, the rate of decrease depending on both the best-estimate warming and the magnitude of uncertainty. For example, there is a 50-70% probability of a wintertime warming of at least 3°C in northern Finland, but further southwest and in the other seasons the probability of so large warming is much smaller (Fig. 5.4).
- An increase in annual mean precipitation from 1961-1990 to 2021-2050 has a high probability in most of the Nordic area, with values ranging from about 80% to nearly 100% (Fig. 5.5). Only in parts and Denmark and Iceland is this probability slightly lower. These values are slightly higher than those reported in RR08 for the central decade (2031-2040) of the same 30-year period, mainly because the uncertainty associated with natural variability is smaller for 30-year than decadal means.
- The sign of precipitation change is most uncertain in summer, when the probability of increase in the Nordic area varies from less than 40% in Denmark and the southern tip of Norway to about 80% in the extreme north.
- Increases of 20% or more in annual precipitation are very unlikely in all of the Nordic area (Fig. 5.6). However, the larger uncertainty in seasonal mean precipitation changes also translates into a somewhat greater probability of large increases, particularly in winter.
- Substantial decreases in precipitation (10% or more) are quite unlikely in northern Europe (Fig. 5.7). Considering the seasonal changes, the probability appears to be largest in western Norway in winter (10-20%) and in Denmark in summer (20-30%).

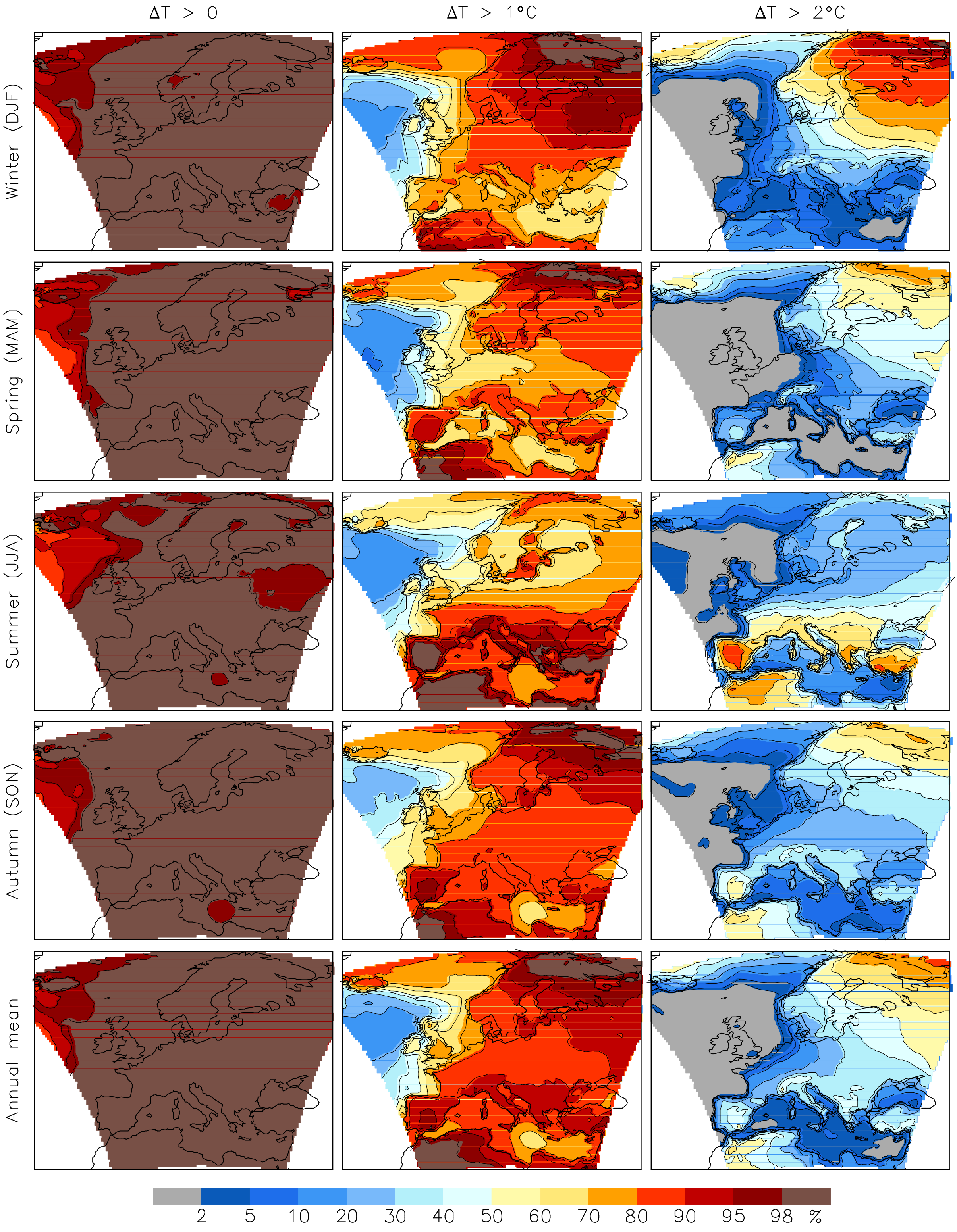

Figure 5.3. *Probability that the temperature change exceeds zero (left), 1°C (middle) and 2°C (right). The colour scale is given below the figure.*

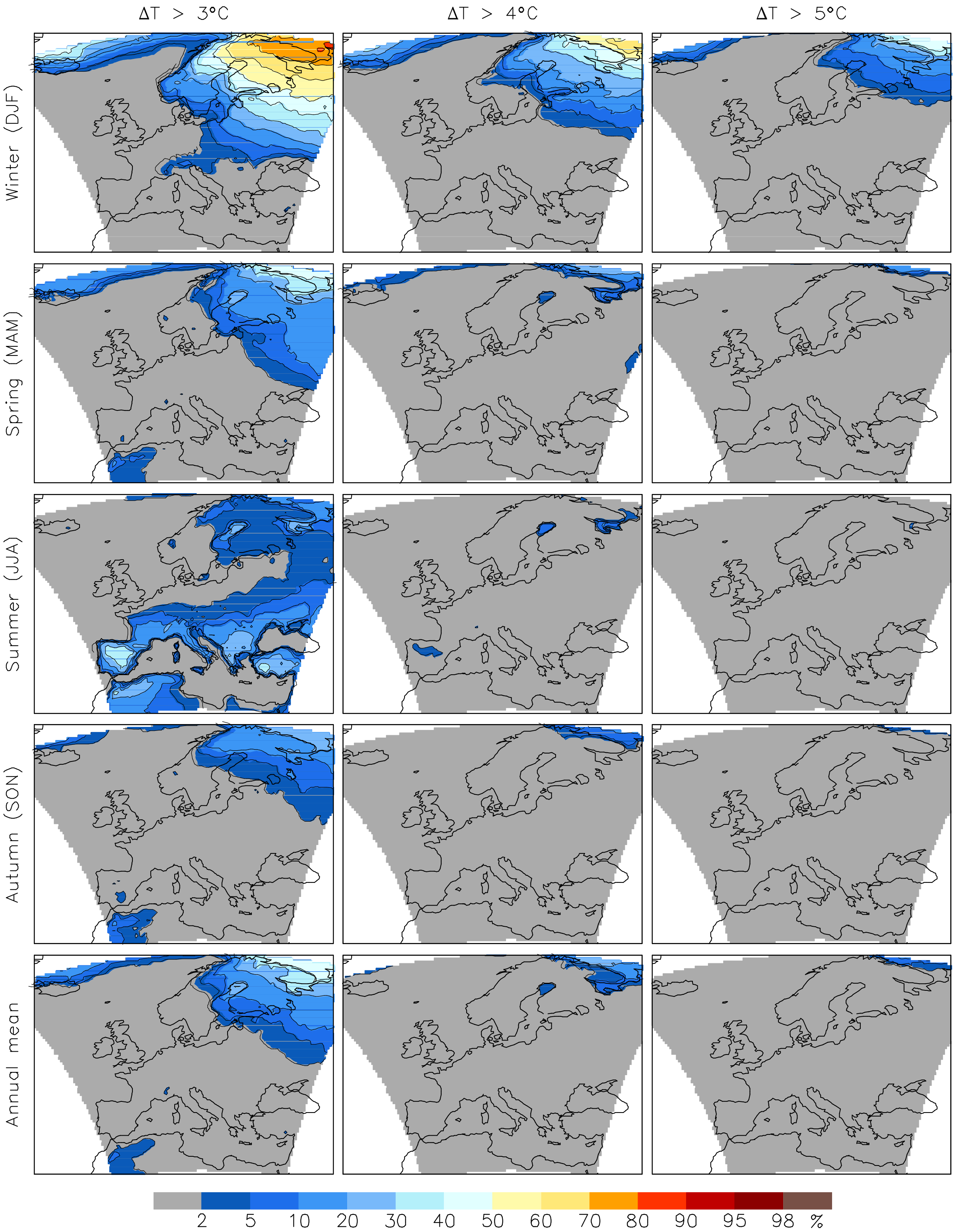

Figure 5.4. *As Figure 5.3, but for thresholds of 3°C (left), 4°C (middle) and 5°C (right).*

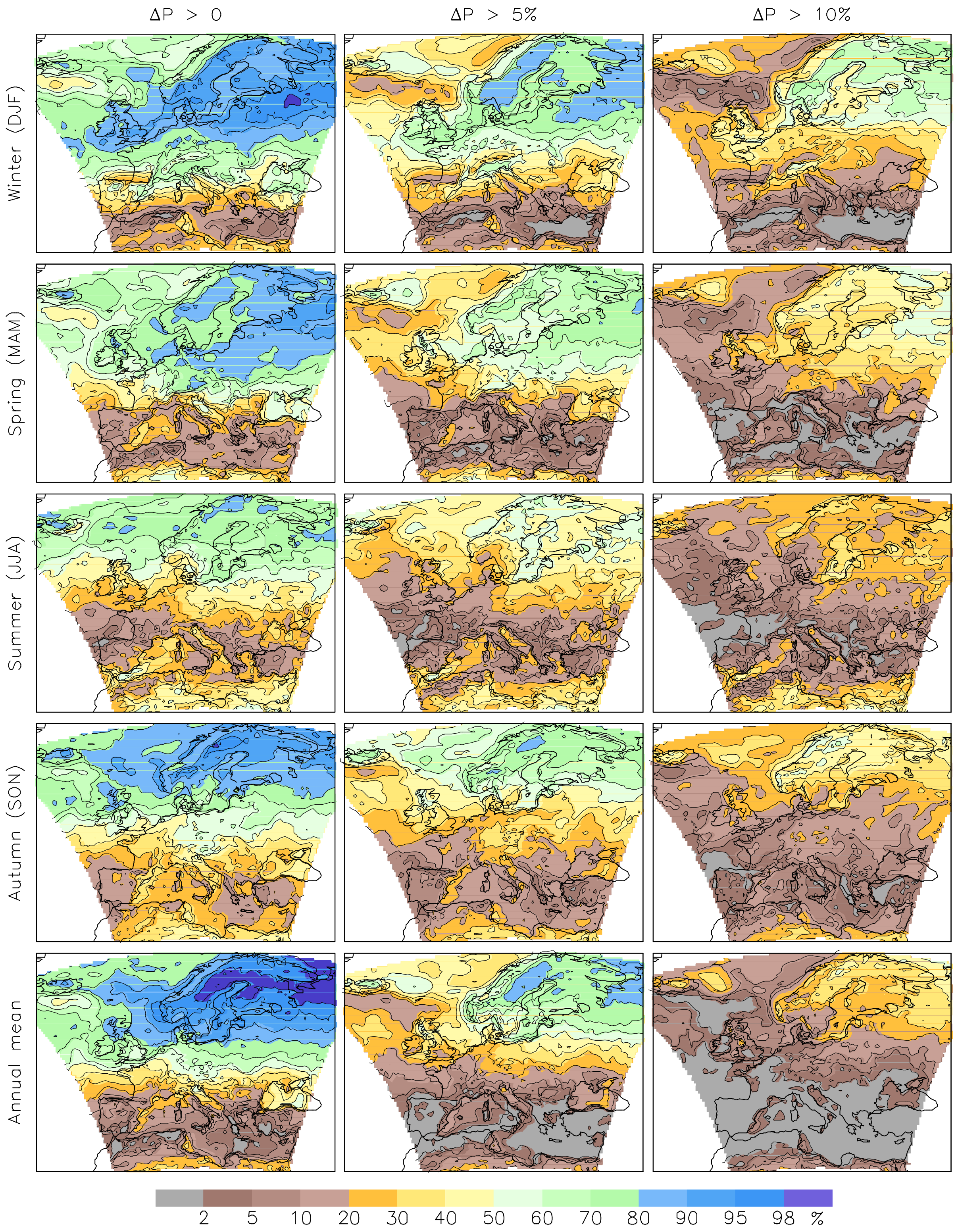

Figure 5.5. *Probability that precipitation increases at least 0% (left), 5% (middle) and 10% (right). The colour scale is given below the figure.*

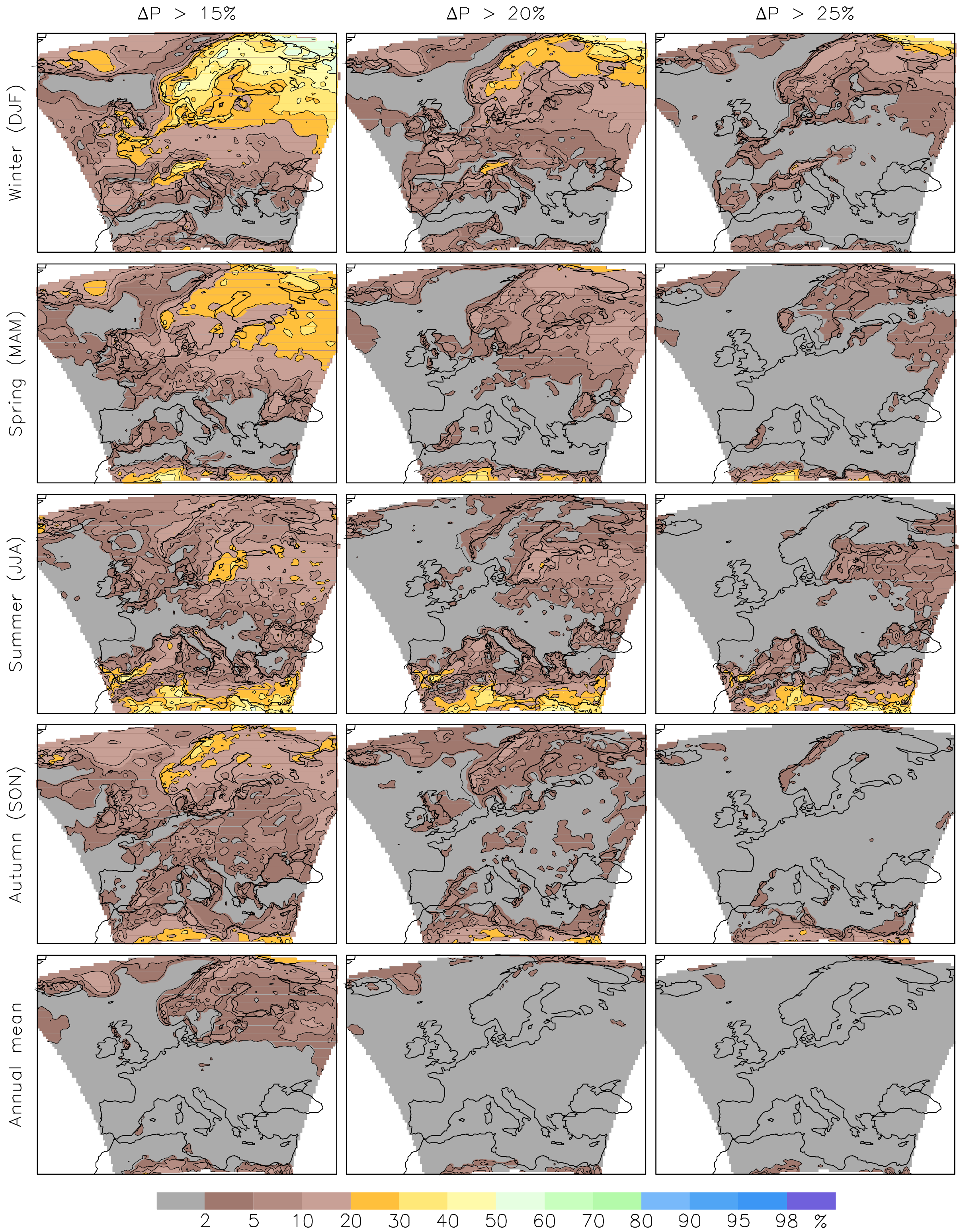

Figure 5.6. *As Figure 5.5, but for precipitation increases of at least 15% (left), 20% (middle) and 25% (right).*

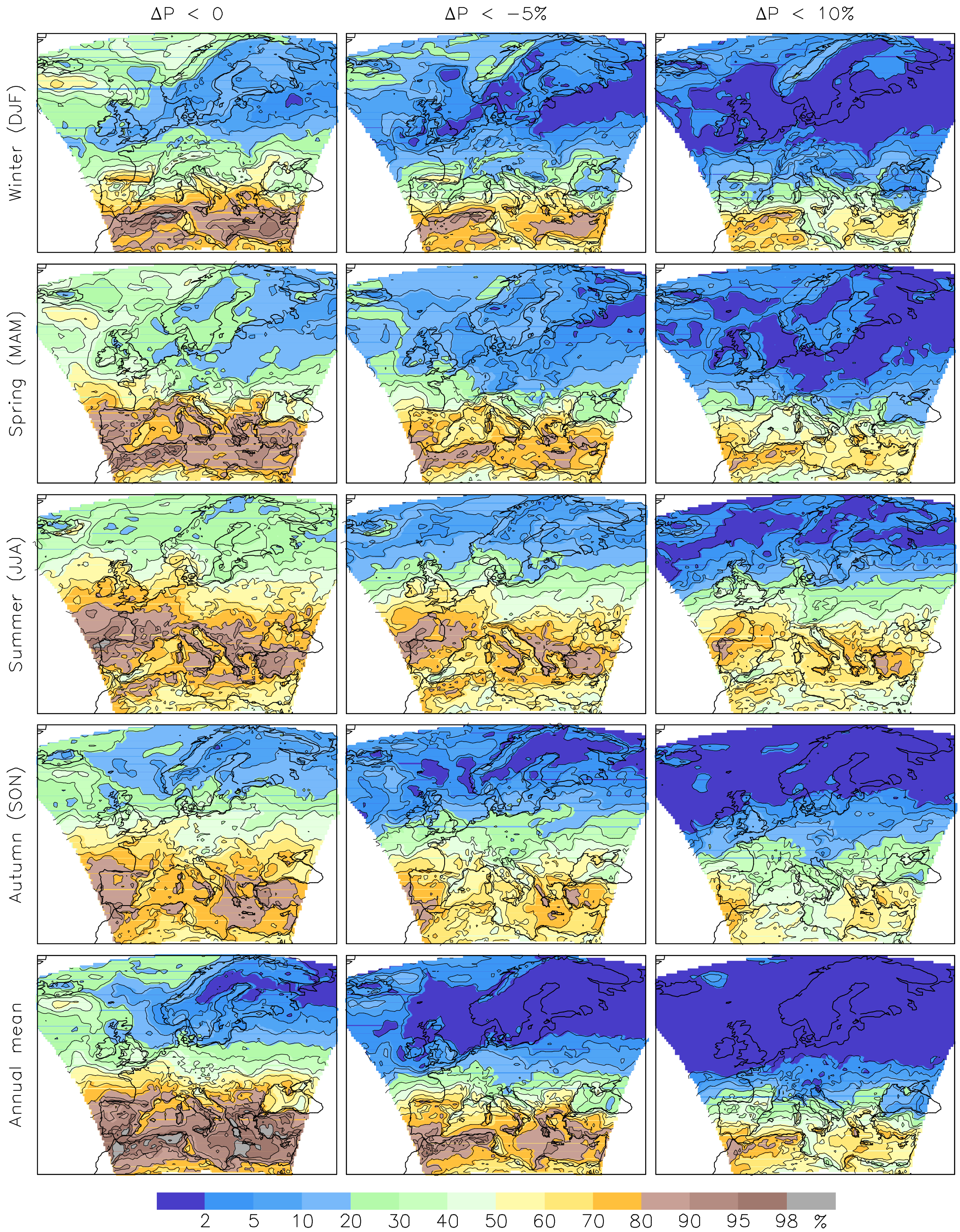

Figure 5.7. *As Figure 5.5, but for precipitation decreases of at least zero (left), 5% (middle) and 10% (right). The colour scale is reversed from the two previous figures.*

6. Conclusions

We have presented in this report probabilistic projections of temperature and precipitation change for northern Europe, focusing on changes from the baseline period 1961-1990 to the forecast period 2021-2050. These projections take into account the uncertainties due to natural climate variability and differences between climate models that dominate the uncertainty of climate change in the early 21st century. Emission scenario uncertainty was not considered, since this has been found to be a secondary issue on this time scale (e.g., Räisänen and Ruosteenoja 2008).

Our projections combine information from 19 global climate model (GCM) and 13 regional climate model (RCM) simulations. The higher resolution of the RCMs adds some physically credible detail to the projections. In particular, land-sea contrasts in temperature change and the effects of orography on precipitation change are both better resolved. On the whole, however, the projections obtained by combining the two data sources are remarkably similar to those obtained by using GCM data alone. The findings from our earlier GCM-based analysis (Räisänen and Ruosteenoja 2008) remain therefore largely valid. Specifically, we find that

- The ongoing increase in atmospheric greenhouse gas concentrations is expected to lead to widespread warming and an increase in precipitation in the Nordic area.
- As the best estimate, the annual mean temperatures in 2021-2050 are projected to exceed the mean of 1961-1990 by about 1.5°C in Iceland, Denmark and the west coast of Norway. In northeastern Fennoscandia, a best-estimate warming of 2-2.5°C is projected.
- The best-estimate projection of annual mean precipitation change suggests an increase of 5-10% in most of the Nordic area.
- Changes in climate vary with season. Largest increases in temperature and (in most of the Nordic area) precipitation are likely to occur in winter.
- Simulated precipitation changes show a marked contrast between an increase in northern and a decrease in southern Europe. The borderline between increasing and decreasing precipitation is in its northernmost position in summer, when precipitation is likely to decrease in parts of southern Scandinavia but increase further north.
- Exact forecasts of future climate change are impossible. However, projections of temperature change are robust in the sense that the sign of the long-term mean change (i.e., warming) is nearly certain.
- Changes in precipitation are relatively more uncertain than those in temperature. In most of the Nordic area, however, an increase of annual mean precipitation has a

probability ranging from 80% to nearly 100%. Changes in summer precipitation are (in terms of the sign) more uncertain than precipitation changes in the other seasons.

- Our analysis suggests a rather large uncertainty for wintertime precipitation changes in western Norway, where precipitation is particularly sensitive to changes in atmospheric circulation.
- Even in the case of temperature, there is a lot of uncertainty in the magnitude of the future change. Similarly to the best-estimate warming, the uncertainty range of temperature change is widest in winter.

Finally, we stress that the analysis in this report relates to the 30-year means of temperature and precipitation in 2021-2050. Because of the projected continuous increase in greenhouse gas forcing, climate changes are likely to grow gradually larger during this period. An analysis of the model simulations suggests that, as the best estimate, temperature and precipitation changes for the decade 2021-2030 should be about 25% smaller, and those for the decade 2041-2050 about 25% larger, than those reported here. Furthermore, weather conditions will vary from year to year, as they have done this far. Thus, for example, some individual cold winters or cool summers are still likely to occur, although their frequency becomes gradually smaller (e.g., Räisänen and Ruokolainen 2008). This issue will be studied later in the CES project.

Acknowledgments

We acknowledge the modeling groups, the Program for Climate Model Diagnosis and Intercomparison (PCMDI) and the WCRP's Working Group on Coupled Modelling (WGCM) for their roles in making available the WCRP CMIP3 multi-model dataset. Support of this dataset is provided by the Office of Science, U.S. Department of Energy. The ENSEMBLES data used in this work was funded by the EU FP6 Integrated Project ENSEMBLES (Contract number 505539) whose support is gratefully acknowledged.

References

Boer, G.J. 2000: A study of atmosphere-ocean predictability on long time scales. *Climate Dynamics*, **16**, 469-472.

Fronzek, S. and TR Carter 2007: Assessing uncertainties in climate change impacts on resource potential for Europe based on projections from RCMs and GCMs. *Climatic Change*, **81**, 357-371.

Hewitt, C.D and Griggs, D.J. 2004: Ensembles-based predictions of climate changes and their impacts. *Eos*, **85**, 566.

IPCC (Intergovernmental Panel on Climate Change) 2007: *Climate Change 2007: the Physical Science Basis*. Cambridge University Press, 996 pp.

Keenlyside, N.S, M. Latif, J. Jungclaus, L. Kornblueh and E. Roeckner 2008: Advancing decadal-scale climate prediction in the North Atlantic sector. *Nature*, **453**, 84-87.

Meehl, G.A., C. Covey, T. Delworth, M. Latif, B. McAvaney, J.F.B. Mitchell, R.J. Stouffer and K.E. Taylor 2007: The WCRP CMIP3 Multimodel Dataset: A New Era in Climate Change Research. *Bulletin of the Americal Meteorological Society*, **88**, 1383-1394.

Mitchell, T.D., T.R. Carter, P.D. Jones, M. Hulme and M. New 2004: A comprehensive set of high-resolution grids of monthly climate for Europe and the globe: the observed record (1901-2000) and 16 scenarios (2001-2100).Tyndall Centre Working Paper 55, 30 pp.

Nakićenović, N. and R. Swart (Eds.) 2000: *Emission Scenarios. A Special Report of Working Group III of the Intergovernmental Panel on Climate Change*. Cambridge University Press, 599 pp.

Räisänen, J., U. Hansson, A. Ullerstig, R. Döscher, L. P. Graham, C. Jones, H. E. M. Meier, P. Samuelsson and U. Willén, 2004: European climate in the late 21st century: regional simulations with two driving global models and two forcing scenarios. *Climate Dynamics*, **22**, 13-31.

Räisänen, J. and L. Ruokolainen 2006: Probabilistic forecasts of near-term climate change based on a resampling ensemble technique. *Tellus*, **58A**, 461-472.

Räisänen, J. and L. Ruokolainen 2008: Estimating present climate in a warming world: a model-based approach. *Climate Dynamics*, **31**, 573-585.

Räisänen, J. and K. Ruosteenoja 2008: Probabilistic forecasts of temperature and precipitation change based on global climate model simulations, 46 pp. Available from http://www.atm.helsinki.fi/~jaraisan/CES_D2.2/CES_D2.2.html

Ruokolainen, L. and J. Räisänen 2007: Probabilistic forecasts of near-term climate change: sensitivity to adjustment of simulated variability and choice of baseline period. *Tellus*, **59A**, 309-320.